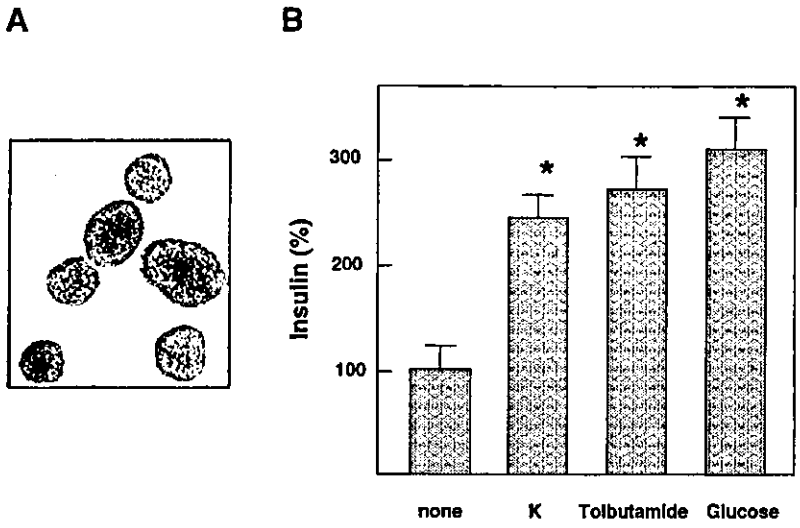

Fig. 3. Insulin Secretion From Pseudoislets
A: Morphology of pseudoislets. Ductal cells were incubated with activin A and BTC for 7 days and pseudoislets were formed as described in Methods. B: Pseudoislets were incubated in KRB buffer containing 50 μM tolbutamide and 16.7 mM glucose for 60 min and insulin released was measured. Values are the mean ± S. E. for four experiments.

Preparation of pseudoislets

We prepared pseudoislets using differentiated cells. Differentiated cells were cultured for 36 to 48 hr in a gelatin-coated dish. Fig. 3A shows the morphology of the pseudoislets. The diameter of pseudoislets was 160 ± 35 μm and the protein content was 1.01 ± 0.08 μg/pseudoislet (n = 5). Fig. 3B shows the insulin secretory response of the pseudoislets. As depicted, insulin secretory response in the pseudoislets was much improved compared to that of the cells cultured in monolayer. Thus, a high concentration of glucose induced more than a three-fold increase in insulin secretion.

Transplantation of pseudoislets

We then transplanted pseudoislets into the portal vein of the STZ-treated nude mice, introducing 50 pseudoislets per mouse. The changes in the plasma glucose concentration are shown in Fig. 4. In STZ-treated mice, the plasma glucose concentration was above 400 mg/dl. Indeed, transplantation of pseudoislets into the portal vein drastically reduced the plasma glucose concentration with the levels of plasma glucose remaining at about 200 mg/dl for at least two weeks.

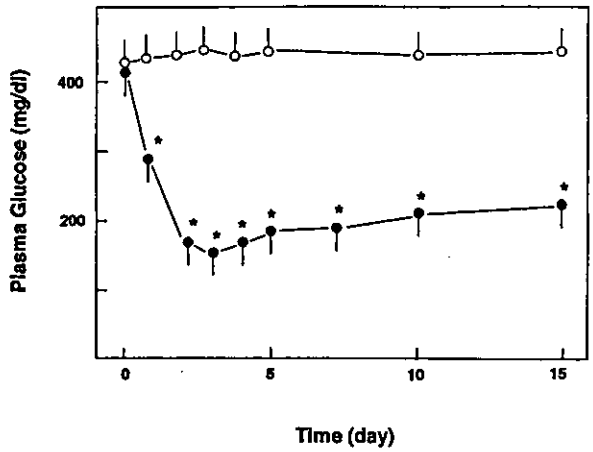

Fig. 4. Changes in the Plasma Glucose Concentration After Transplantation of Pseudoislets
Fifty pseudoislets (●) or saline (○) were injected into the portal vein via the cecal vein of the STZ-treated nude mice. Plasma glucose concentration was measured. Values are the mean ± S. E. for five experiments. *: $p<0.05$ vs control.

Discussion

In the present study, we attempted to induce differentiation of ductal cells and convert them into insulin-secreting cells. Differentiation was achieved by the treatment with two differentiation factors, activin A

and BTC. A combination of these two factors was previously shown to convert amylase-secreting AR42J cells into insulin-producing cells [9] and intraislet precursor cells to β cells [2]. The majority of the differentiated cells expressed insulin, although some of them expressed somatostatin; interestingly, no cells expressed glucagon. Hence, a combination of these two factors may selectively induce differentiation to the β cell lineage. Differentiated cells possessed a regulatory secretion pathway since they were able to secrete insulin in response to a depolarizing concentration of potassium. They also responded to tolbutamide, an inhibitor of the K_{ATP} channel. The latter observation suggests that differentiated cells also express the K_{ATP} channel. More importantly, differentiated cells responded to a high concentration of glucose although the magnitude of the response was not great. Differentiated cells therefore express the machinery necessary for glucose-responsive insulin secretion including GLUT2, glucokinase, the K_{ATP} channel and the voltage-dependent calcium channel. The insulin secretory response to glucose was much improved when differentiated cells formed pseudoislets. Thus, insulin response to high glucose concentration increased more than three-fold. The exact reason for the improved response is not clear, but cell adhesion and subsequent formation of gap junction may be among the causes. Islet β cells express E-cadherin [11] and, when adhered to each other, cells were electrically connected via gap junction. Presumably, β cells in pseudoislets do not simply form a cell cluster but also synchronize in terms of electrical activity as islet cells do [12]. In any case, the formation of pseudoislets is quite effective to obtain β cells with reasonably good secretory response. The formation of pseudoislets is also advantageous for transplantation into the portal vein. Although the exact location of the transplanted pseudoislets in the liver is not known, they certainly are located in the upstream of hepatocytes, a major target of the insulin action. As reported recently [13], the liver has an envivonment supporting the differentiation and survival of pancreatic β cells, and in this sense transplantation into the portal vein is perhaps better than transplantation of islets in the peripheral tissue such as subcutaneous tissue.

In the present study, we established a method for transplantation of β cells obtained from precursor cells in the pancreatic duct. However, some issues remain to be resolved. First of all, a larger number of β cells *in vitro* need to be obtained for transplantation. We obtained approximately 50 pseudoislets using ductal cells obtained from three neonatal rats. If we could stimulate the proliferation of ductal cells more extensively or increase the number of insulin-producing cells during differentiation, more pseudoislets for transplantation could be used. In this regard, a different class of growth or differentiation factor is desirable. Also, better conditions for cultivation should be established. Secondly, although we could convert ductal cells to insulin-secreting β cells and obtained pseudoislets using the latter cells, maturation of the cells was still not high enough. The method for induction of differentiation needs to be improved. Again, a better differentiation factor would be effective to obtain more differentiated β cells. Also, culture conditions including extracellular matrix may be important. Thirdly, optimization of the conditions for transplantation is necessary. In particular, we really do not know yet how many pseudoislets are necessary to maintain normoglycemia for a long period. In human islet transplantation, the number of islets transplanted is a critical factor and a large number of islets provides a better outcome [5]. In this regard, the examination of the effect of transplantation using a greater number of pseudoislets is vital. Further studies are necessary to resolve these issues.

Acknowledgments

The present study was supported by a grant from the Project for Realization of Regenerative Medicine and a Grant for Scientific Research from the Ministry of Education, Science, Sports and Culture of Japan. The authors are grateful to Mayumi Odagiri for technical and secretarial assistance.

References

1. Bonner-Weir S (2000) Islet growth and development in the adult. *J Mol Endocrinol* 24: 297–302.
2. Zulewski H, Abraham EJ, Gerlach MJ, Daniel P, Moritz W, Muller B, Vallejo M, Thomas MK, Harbener

JF (2000) Multipotential Nestin-positive stem cells isolated from adult pancreatic islets differentiate ex vivo into pancreatic endocrine, exocrine and hepatic phenotypes. *Diabetes* 50: 521–533.
3. Ramiya VK, Maraist M, Arfors KE, Schatz DA, Peck AB, Cornelius JG (2000) Reversal of insulin-dependent diabetes using islets generated in vitro from pancreatic stem cells. *Nature Med* 6: 278–282.
4. Bonner-Weir S, Taneja M, Weir GC, Tatarkiewicz K, Song KH, Sharma A, O'Neil JJ (2000) In vitro cultivation of human islets from expanded ductal tissue. *Proc Natl Acad Sci USA* 97: 7999–8004.
5. Shapiro AMJ, Lakey JRT, Ryan EA, Korbutt GS, Toth E, Warnock GL, Kheteman NM, Rajotte RV (2000) Islet transplantation in seven patients with type I diabetes mellitus using a glucocorticoid-free immunosuppressive regimen. *N Engl J Med* 343: 230–238.
6. Seno M, Tada H, Kosaka M, Sasada R, Igarashi K, Shing Y, Falkman J, Ueda M, Yamada H (1996) Human betacellulin, a member of the EGF family, dominantly expressed in pancreas and small intestine, is fully active in a monomeric form. *Growth Fact* 13: 181–191.
7. Zhang YQ, Zhang H, Maeshima A, Kurihara H, Miyagawa J, Takeuchi T, Kojima I (2002) Up-regulation of the expression of activins in the pancreatic duct by reduction of the β cell mass. *Endocrinology* 143: 3540–3547.
8. Zhang YQ, Mashima H, Kojima I (2001) Changes in the expression of transcription factors in pancreatic AR42J cells during differentiation into insulin-producing cells. *Diabetes* 50: S10–S14.
9. Mashima H, Ohnishi H, Wakabayashi K, Miyagawa J, Hanafusa T, Kojima I (1996) Betacellulin and activin A coordinately convert amylase-secreting AR42J cells into insulin-secreting cells. *J Clin Invest* 97: 1647–1654.
10. Yokoyama-Hayashi K, Takahashi T, Kakita A, Yamashina S (2002) Expression of PGP9.5 in ductal cells of the rat pancreas during development and regeneration. *Endocr J* 49: 61–74.
11. Moller CJ, Christgau S, Williamson MR, Madsen OD, Niu ZP, Bock E, Baekeskov S (1992) Differential expression of neural cell adhesion molecule and cadherins in pancreatic islets, glucagonomas and insulinomas. *Mol Endocrinol* 6: 1332–1342.
12. Hauge-Evans AC, Aquires PE, Persaud SJ, Jones PM (1999) Pancreatic beta-cell-to-beta-cell interactions are required for integrated responses to nutrient stimuli. *Diabetes* 48: 1402–1408.
13. Kojima H, Fujimiya M, Matsumura K, Younan P, Imaeda H, Maeda M, Chan L (2003) Neuro-D-beta-cellulin gene induces islet neogenesis in the liver and reverses diabetes in mice. *Nature Med* 5: 596–673.

FEBS 28465 FEBS Letters 568 (2004) 39–43

Insertional-fusion of basic fibroblast growth factor endowed ribonuclease 1 with enhanced cytotoxicity by steric blockade of inhibitor interaction

Hiroko Tada*, Masayuki Onizuka, Kazuko Muraki, Wataru Masuzawa, Junichiro Futami, Megumi Kosaka, Masaharu Seno, Hidenori Yamada

Department of Bioscience and Biotechnology, Faculty of Engineering, Graduate School of Natural Science and Technology, Okayama University, Okayama 700-8530, Japan

Received 27 February 2004; revised 30 April 2004; accepted 6 May 2004

Available online 18 May 2004

Edited by Takashi Gojobori

Abstract **Basic fibroblast growth factor (bFGF) was inserted in the middle of human ribonuclease 1 (RNase1) sequence at an RNase inhibitor (RI)-binding site (Gly89) by a new gene fusion technique, insertional-fusion. The resultant insertional-fusion protein (CL-RFN89) was active both as bFGF and as RNase. Furthermore, it acquired an additional ability of evading RI through steric blockade of RI-binding caused by fused bFGF domain. As a result, CL-RFN89 showed stronger growth inhibition on B16/BL6 melanoma cells than an RI-sensitive tandem fusion protein. Thus, the insertional-fusion technique increases accessible positions for gene fusion on RNase, resulting in construction of a potent cytotoxic RNase.**

Keywords: Ribonuclease; Basic fibroblast growth factor; Insertional-fusion protein; Targeting; Protein engineering

1. Introduction

Several kinds of hybrid proteins have been constructed to produce bifunctional proteins and utilized as tools such as detectors for biological molecules. Generally, those hybrid proteins have been built by end-to-end fusion (tandem-fusion) of two genes of component proteins. The alternative is to insert the second protein (the insert protein) into the middle of the sequence of the host protein in-frame [1,2]. This new mode of gene fusion (insertional-fusion) is expected to give an additional configuration between two component domains and to make it possible to create the hybrid protein with the ideal 3D structure for new functions. However, the insertional-fusion has not been popular because it is apparently more limited and requires precise information on the parental protein structures. Therefore, insertional-fusion has first been achieved by random screening to find accessible site for insert sequences [3]. Recently, it has been suggested that the tolerance of protein structures to very large protein insertions is more general than previously thought [4], and some insertional-fusion proteins have been designed based on the 3D structures of component proteins and successfully obtained in active structures. However, the resultant proteins were less stable than the parental proteins (reviewed in [2]).

We used this insertional-fusion technique for engineering human RNase1 to be cytotoxic. RNase1 itself is not cytotoxic as a majority of RNase superfamily. The major reasons considered for it are (1) the neutralization of their ribonucleolytic activity by RNase inhibitor (RI) expressed ubiquitously in the cytosol [5], and (2) insufficient binding to the target cells. Therefore, engineered variants of RNase1, which could efficiently reach the cytosol of the target cells [6,7] and/or to maintain their activity there by evading the action of RI [8], were reported to acquire cytotoxicity. Previously, we constructed cytotoxic RNase by fusing human basic fibroblast growth factor (bFGF) to the C-terminus of RNase1 [9]. The resultant tandem-fusion protein (RNF) could inhibit the growth of malignant cells with high levels of cell surface FGF receptor. However, its activity was still weak (IC_{50} value was more than 1 μM) probably because it could not evade inactivation by RI.

In this study, bFGF was inserted into RNase1 at the exact RI-binding site that is in the middle of RNase sequence. The resultant insertional-fusion protein had both abilities of efficient binding to target cells and evading RI by masking the RI interaction site with the targeting protein of bFGF. Furthermore, an additional intramolecular disulfide-bridge was introduced in the insertional-fusion protein to increase its conformational stability that was suggested as another important determinant of RNase-mediated cytotoxicity [10,11]. These insertional-fusion proteins were evaluated for activities of both RNase and bFGF, for stability against protease digestion, and for growth inhibition on malignant cells.

* Corresponding author. Fax: +81-86-251-8265/8216.
E-mail address: tadahrk@biotech.okayama-u.ac.jp (H. Tada).

Abbreviations: bFGF, basic fibroblast growth factor; CL-RNase1, 4-118 cross-linked RNase1 mutant; RFNs, insertional-fusion proteins between hRNase1 and bFGF; CL-RFNs, insertional-fusion proteins between CL-RNase1 and bFGF; RI, ribonuclease inhibitor

2. Materials and methods

2.1. Materials

Recombinant human RNase1, 4–118 cross-linked RNase 1 (CL-RNase 1) and human bFGF (147 amino acid form) were purified from *Escherichia coli* as described previously [9,12].

0014-5793/$22.00
doi:10.1016/j.febslet.2004.05.007

2.2. Construction of insertional-fusion proteins

A cDNA encoding bFGF (19–146) (N-terminal 18 residue-truncated form of bFGF) was amplified by polymerase chain reaction using primers (5′-TTTCCGCGGGCAGCGACCCCAAGCGGCTGTAC-3′) and 5′-ATTCCGCGGAGCTTTCAGCAGACATTGG-3′) and pBO126 [9] as a template. On the other hand, a *Sac*II site was introduced at the position of Pro19 or Gly89 of RNase1 cDNA into an RNase1 expression vector of pBO26 [13] by site-directed mutagenesis. The resultant plasmids were cleaved with *Sac*II and ligated in-frame with the *Sac*II fragment of bFGF (19–146) to construct the expression vectors for insertional-fusion proteins with bFGF insertion at Pro19 (RFN19) or at Gly89 (RFN89) of RNase1, respectively. Similarly, the expression vectors for fusion proteins with bFGF (19–146) insertion at Pro19 (CL-RFN19) or at Gly89 (CL-RFN89) of CL-RNase1 were constructed using an expression vector for CL-RNase1, pBO383 [12], instead of pBO26. The expression vector for an insertional-fusion protein with bFGF (21–144) insertion at Gly89 of CL-RNase1 (CL-RFN89-2) was also constructed by insertion of the bFGF (21–144) fragment amplified with primers (5′-ATACCGCGGCCAAGCG-GCTGTAC-3′ and 5′-AGCCCGCGGCAGACATTGGAAG-3′). The schematic structures of these RFNs and CL-RFNs are depicted in Fig. 1A.

2.3. Expression, refolding and purification of insertional-fusion proteins

All of the insertional-fusion and tandem-fusion proteins were expressed as inclusion bodies in *E. coli*, and then solubilized, refolded, and purified by the same procedure as described previously [13,14]. The purified proteins were concentrated by ultrafiltration with Ultrafree-4 centrifugal filter (Biomax-5K NMWL, Millipore, USA). Protein concentrations were determined by UV spectroscopy as described [15].

2.4. Assays for RNase activity

Ribonucleolytic activity of the insertional-fusion proteins on yeast transfer RNA was measured as described previously [16]. To evaluate the affinity of RI for each protein, their RNase activity was measured in the presence and absence of 130 units/ml of recombinant human placental RI (Wako, Japan) (1 unit of RI is that amount required to inhibit 50% the activity of 5 ng of RNase A) and 1 mM DTT.

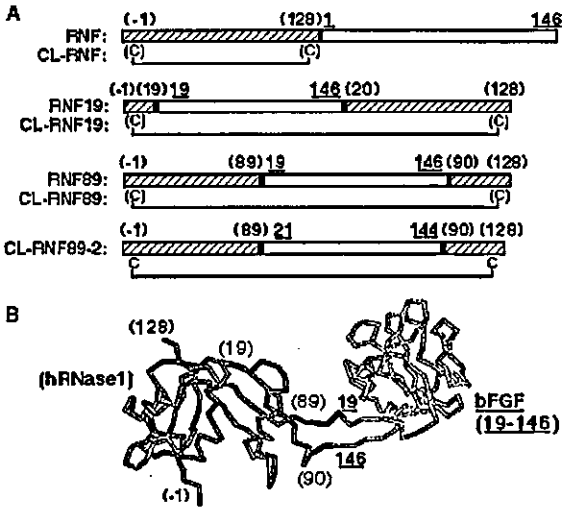

Fig. 1. The schematic structures of insertional-fusion proteins between bFGF and RNase1. (A) The bFGF (white bar) was inserted in host RNase1 (striped bar) by gene fusion. Black bars indicate linker sequences derived from restriction sites for insertion. The positions of additional disulfide cross-link and introduced cystein residues are shown. (B) Model of CL-RFN89. The structure derived from RNase1 (PDB No. 1UFS, unpublished data) is dark gray and that from bFGF (PDB No. 2FGF [27]) is light gray. This figure was produced using the RasMac molecular graphics program, version 2.6 [28]. The amino acid residue numbers derived from RNase1 sequence are indicated in parenthesis and those from bFGF are underlined. Extra methionine residues at −1 positions of these proteins derived from the initiation codons were all confirmed by N-terminal amino acid sequence analysis, and indicated as (−1).

2.5. Mitogenic activity toward serum-starved murine fibroblasts

Mouse Balb/c 3T3 A31 cells were grown in Dulbecco's modified Eagle's medium (DMEM; Nissui, Japan) containing 10% fetal bovine serum (FBS). The cells were plated onto 96-well plates (1.5×10^3 cells/well) and cultured for 12h. The medium was then replaced with DMEM containing 0.5% FBS (100 μl) and the cells were incubated for 1 day to starve the cells. Then, 100 μl of samples was added to the wells. After 2 days of cultivation, the cell growth was measured with 3-(4,5-dimethylthiazol-2-yl)-2,5-diphenyltetrazolium bromide (MTT) as described previously [17].

2.6. Assays for growth inhibitory effect

Cytotoxicity on mouse metastatic melanoma B16/BL6 cells was evaluated as described previously [9].

2.7. Tryptic digestion

Digestion of each protein was carried out under the physiological conditions with trypsin [12]. Five μg of proteins dissolved in 15 μl of 75 mM Tris–HCl, pH 8.0, was incubated with indicated concentrations of TPCK-trypsin at 37 °C for 30 min. The reactions were stopped by addition of a sample buffer and analyzed by SDS–PAGE on 15% polyacrylamide gel under reducing conditions.

3. Results and discussion

3.1. Design of insertional-fusion proteins between RNase1 and bFGF

Previous studies on native cytotoxic RNases as well as engineered cytotoxic RNases have shown that the mechanism of RNase-mediated cytotoxicity consists of two steps: binding to the target cells to reach cytosol and catalytic cleavage of cellular RNA. If a targeting protein can be fused at the exact site of RI-binding on the RNase1 molecule, the resultant fusion protein is expected to show cytotoxicity through both abilities of efficient cell binding and efficient ribonucleolytic activity in the cytosol in which RI is ubiquitously expressed. However, it is impossible to construct such a structure by the conventional tandem-fusion technique, because both termini of RNase are apart from the RI-binding sites. Previously, Suzuki et al. conjugated a targeting protein (transferrin) with RNase1 at the RI-binding site via a thioether bond [18] with an aim similar to ours and successfully obtained a cytotoxic RNase. In this study, we used insertional-fusion technique to place a targeting protein at the RI-binding site. On the design of insertional-fusion proteins, we selected bFGF as a targeting protein for insertion, since the N- and C-termini of "beta-trefoil core region (residues 19–146)" of bFGF are near each other (5.3 Å between Cαs of Asp19 and Lys145) as shown in Fig. 1B. This fragment has been shown to be sufficient for its biological activities [19]. On the other hand, an RI-binding site of Gly89 [20] was selected as the insertion site on RNase1. Pro19 irrelevant to RI-binding was also selected as another insertion site for control. Taken together, we constructed two insertional-fusion proteins of RFN89 and RFN19, respectively (Fig. 1A). Furthermore, we constructed two additional insertional-fusion proteins named CL-RFN89 and CL-RFN19 using a stabilized mutant of RNase1 (CL-RNase1) as a host, to obtain more stable insertional-fusion proteins. In CL-RNase1, two cystein residues introduced at positions 4 and 118 of RNase1 form an additional intramolecular disulfide cross-link to stabilize its structure [12]. Furthermore, CL-RFN89-2 was constructed by inserting bFGF

(21–144) sequence at Gly89 of CL-RNase1 to shorten linker sequences.

3.2. Activities of RNase domain and bFGF domain of insertional-fusion proteins

When these insertional-fusion proteins were expressed directly in *E. coli*, they were produced as inclusion bodies. After refolding, the yields of all the insertional-fusion proteins purified from 1 liter-culture were about the same, from 5 to 10 mg. As shown in Table 1, all of these insertional-fusion proteins were ribonucleolytically active (30% or more of wild-type RNase1). The results indicate that their RNase domains were properly folded as the parental RNase1, nevertheless their primary sequences are divided and intervened by long bFGF sequence.

To access their actual activity under cytosolic conditions, RNase activity was measured in the presence of RI (Fig. 2). RNase activity of RFN19, CL-RFN19, and RNF was completely inhibited by RI as RNase1 was. In contrast, RFN89, CL-RFN89, and CL-RFN89-2 retained their activity by 85% or more even in the presence of 200-fold molar excess amount of RI. From these results, the values of inhibitor constant (K_i) of RFN89, CL-RFN89 and CL-RFN89-2 to RI were estimated to be approximately 100–200 nM (Table 1), which were 10^4-fold higher than that of wild-type RNase1 ($K_i = 20$ pM [21]). Thus, the insertional-fusion proteins with bFGF insertion at the RI-binding site of RNase1 acquired the ability of evading RI.

Mitogenic activity of these insertional-fusions was accessed to evaluate the activity of bFGF domain (Table 1). All the insertional-fusion proteins showed strong mitogenic activity as much as the tandem RNF. Thus, the bFGF domain is also properly folded in the middle of RNase1 sequence to bind cell-surface FGF-receptors.

3.3. Stability of insertional-fusion proteins against tryptic digestion

The conformational stability of RNases was suggested as another important factor for their cytotoxic activity [10,11]. However, in general, "insertional-fusion proteins" have been shown to be less stable than the parental proteins [4]. In the case of another insertional-fusion protein between SH3 domain and protein L, the free energy for unfolding of SH3 was

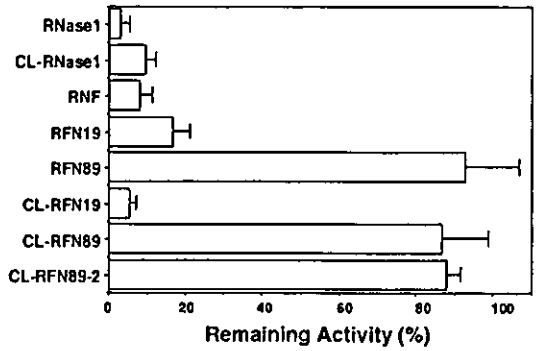

Fig. 2. Enzymatic activity of the insertional-fusion proteins in the presence of RI. Inhibition of ribonucleolytic activity of the insertional-fusion proteins by RI was assayed with tRNA as a substrate. Remaining activity (%) is indicated as relative activity in the presence of RI (a molar ratio of enzyme to inhibitor of 1:200–300) to that in the absence of RI. The values were means ± S.D. of three experiments.

reported to be reduced by 1.2 kcal/mol [22]. We therefore evaluated the stability of the insertional-fusion proteins by tryptic digestion. As shown in Fig. 3, the insertional-fusion proteins were digested faster than the tandem-RNF and parental RNase1, indicating that their structures are considerably destabilized. RFN89 was less stable than RFN19 in spite of same length and sequence of the insert, suggesting that some significant destabilization such as conformational strain might be associated with RFN89. Thus, although RFN89 was obtained as active form, it was considered to be too unstable to resist proteolytic digestion systems in the target cells. CL-RFNs, in which an additional intramolecular disulfide-bridge was introduced to stabilize their structure, were more stable than the respective RFNs, although they were still less stable than the tandem-RNF. As another attempt, both of the spacer sequences between host and insert domains were shortened by two residues in CL-RFN89-2 (Fig. 1A), however, obvious additional stabilization or destabilization was not observed in the tryptic digestion assay (data not shown). Similar results were obtained by using proteinase K instead of trypsin, suggesting that the increased protease-sensitivity was not sequence specific but resulted from the decreased conformational stability of these fusion proteins because protease digestion of small globular proteins generally occurs from the unfolded

Table 1
Characteristic properties of the insertional-fusion proteins between RNase1 and bFGF

Proteins	RNase activity (%)[a]	Inhibitor constant K_i (nM)[b]	Mitogenic activity ED_{50} (pM)[c]	Growth inhibition IC_{50} (μM)[d]
RNF	84.8 ± 3.5	2.1 ± 0.8	18.6 ± 16.5	1.6 ± 0.8
RFN19	50.2 ± 3.2	4.7 ± 1.4	9.5 ± 6.8	1.5 ± 1.1
RFN89	68.2 ± 9.1	1.3 ± 0.3	26.0 ± 15.3	0.87 ± 0.30
CL-RFN19	76.0 ± 7.4	118 ± 9.8	8.7 ± 5.4	>3
CL-RFN89	36.8 ± 4.6	110 ± 51	6.7 ± 3.0	0.32 ± 0.14
CL-RFN89-2	33.1 ± 1.5	193 ± 34	5.5 ± 4.0	0.23 ± 0.17
HRNase1	100	<1	n.d.[e]	n.d.[e]
CL-RNase	38.9 ± 1.8	1.8 ± 0.8	n.d.[e]	n.d.[e]
bFGF	–	–	118 ± 85	>3

[a] Ribonucleolytic activity was measured at 37 °C by using yeast transfer RNA as a substrate and expressed as relative activity (%) to that of RNase1.
[b] Inhibitor constant to RI was calculated from the data shown in Fig. 2, as described previously [16].
[c] Mouse fibroblast Balb/c 3T3 A31 cells were cultured with various proteins under low-serum (0.5%) conditions. After 3 days, the cell growth was measured by the MTT assay.
[d] Mouse B16/BL6 melanoma cells were cultured with various proteins for 3 days. The growth of the cells was measured by the MTT assay.
[e] Not detected.

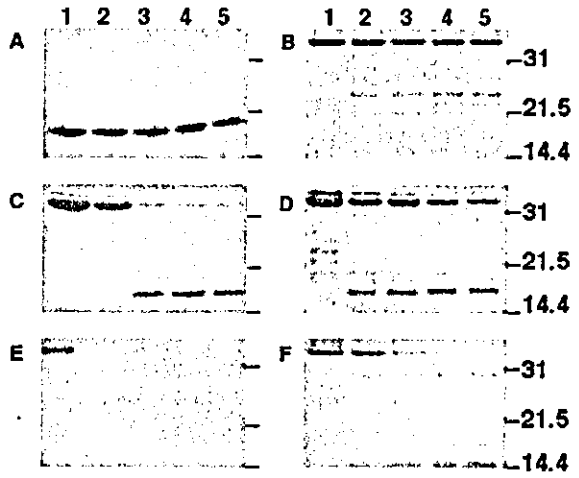

Fig. 3. SDS–PAGE analysis of digestion of the insertional-fusion proteins with trypsin under physiological conditions. The insertional-fusion proteins were incubated in the presence of various concentrations of trypsin at pH 8.0 and 37 °C for 30 min, and then subjected to SDS–PAGE. The concentrations of trypsin were 0 μg/ml (lane 1), 0.5 μg/ml (lane2), 1.0 μg/ml (lane 3), 2.1μg/ml (lane 4), and 4.2 μg/ml (lane 5), respectively. Panels A, hRNasel; B, RNF; C, RFN19; D, CL-RFN19; E, RFN89; F, CL-RFN89, respectively. Bars on the right show the positions of some molecular protein size markers.

state in the unfolding equilibrium as described previously [23,24]. The results from the N-terminal sequence analysis of the partially digested fragments of the RFNs indicated that the host domain was much less stable than the insert domain and thus the digestion occurred preferentially in the host domain (data not shown). This suggested that the host domain (RNase) was preferentially destabilized in the RFNs. Although the insert domain was also destabilized to be digested faster than bFGF itself, the effect to the host domain is considered more significant than the insert domain. Considering the unstable nature of RFN89, RNasel is thought to have only enough conformational stability (5.7 kcal/mol [12]) to tolerate insertional-fusion. On the other hand, when an intramolecular disulfide-bridge was introduced in RNasel, the conformational stability of the resultant mutant of CL-RNasel increased by approximately 2 kcal/mol [12]. These observations suggest that introduction of additional intramolecular disulfide bridges would be a general and effective strategy against destabilization associated with insertional-fusion.

3.4. Growth inhibition by insertional-fusion proteins

All of the insertional-fusion proteins except CL-RFN19 inhibited the growth of B16/BL6 melanoma cells similar to the tandem-fusion protein RNF (Table 1). As expected, the activity of the insertional-fusion proteins with higher stability and RI-evading ability (CL-RFN89 and CL-RFN89-2) was 5- and 7-fold stronger than that of RNF, respectively. In contrast, RI-sensitive CL-RFN19 showed little growth inhibitory effect, although it was more stable and more ribonucleolytically active in the absence of RI than RI-resistant ones.

In this study, we measured four factors possibly involved in the growth inhibitory effect of the fusion proteins between RNasel and bFGF: RNase activity itself derived from RNase domain, that in the presence of RI, the mitogenic activity derived from bFGF domain, and the stability against proteases. Among them, the RNase activity in the presence of RI as a result of the RI-evading ability was indicated as the most important factor for the growth inhibition. The facts that the difference in the inhibitor constant (K_i) values among the fusion proteins (more than 100 nM for RI-evading CL-RFN89s and less than 5 nM for other RI-sensitive fusion proteins) was remarkable and the value was relatively close to their IC50 values might be the reasons for the effectiveness (Table 1). In addition, the structural stability was also suggested to affect the growth inhibitory activity since the increase in growth inhibitory activity of the least stable RFN89 was only slight, although it showed highest RNase activity in the presence of RI. These results suggested that the effect of enhanced RNase activity in the presence of RI was almost completely cancelled by the rapid decrease of the actual concentration of active RFN89 in the cells caused by the rapid degradation of unstable RFN89. In contrast, intrinsic RNase activity is considered to have little effect on the present growth inhibition, because the enhancement of RI-evading was more prominent than the decrease in RNase activity of the fusion proteins (Table 1 and Fig. 2). As for the targeting ability derived from bFGF, the lower ED50 values in the mitogenic activity of the fusion proteins suggested their higher affinity to high affinity tyrosine-kinase receptors for bFGF but their similar elution profile on heparin-column HPLC (data not shown) suggested that their affinity to low-affinity receptors would be equivalent to that of bFGF. However, this targeting ability also had little effect on the growth inhibition. The ED_{50} values of mitogenic activity (from 0.005 to 0.03 nM) as well as reported affinity of bFGF to their cell surface receptors (K_d of 0.2 nM for high-affinity receptors and 9 nM for low-affinity receptors [25]) were extremely lower than the IC_{50} values of their growth inhibition

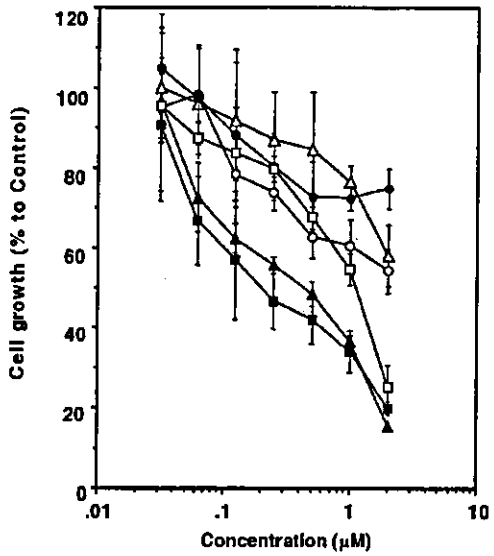

Fig. 4. Growth inhibitory effects of the insertional fusion proteins on mouse melanoma B16/BL6 cells. B16/BL6 cells (5×10^2 cells/well) were cultured for 3 days with RNF (open triangle), RFN19 (open circle), RFN89 (open square), CL-RFN19 (solid circle), CL-RFN89 (solid triangle), and CL-RFN89-2 (solid square), respectively. Cell growth of each well was monitored by MTT assay. Each point and vertical line show the mean value and the S.D. of triplicates, respectively.

(more than 200 nM), suggesting that all of the fusion proteins already had sufficient affinity for their receptors (see Fig. 4).

Considering CL-RFN89 as an anti-cancer cytotoxin, use of growth factors such as bFGF as a targeting carrier may be controversial, because it might be possible that their mitogenic effect could cancel their growth inhibitory effect or cause the proliferation of the target cancer and/or the normal cells in vivo. Although little mitogenic effect was observed on Balb/c 3T3 cells as well as B16/BL6 melanoma cells in the normal culture containing 10% serum (data not shown), this possibility of CL-RFN89 should be checked by using the individual target cancer cells as well as normal tissues before therapeutic application. This problem will be solved by using antagonistic bFGF mutants that possess decreased mitogenicity with little change in affinity for cell surface receptors [26]. Since CL-RFN89 also inhibits the proliferation of other FGFR-positive cells such as human vein endothelial cells, the possibility of its therapeutic application to neovascular diseases is now under investigation.

Acknowledgements: This work was partly supported by a Grant-in-Aid for Okayama Foundation for Science and Technology and a Grand-in-Aid for Scientific Research from the Ministry of Education, Science, Sports and Culture of Japan.

References

[1] Russell, R.B. (1994) Protein Eng. 7, 1407–1410.
[2] Doi, N. and Yanagawa, H. (1999) FEBS Lett. 457, 1–4.
[3] Biondi, R.M., Baehler, P.J., Reymond, C.D. and Veron, M. (1998) Nucleic Acids Res. 26, 4946–4952.
[4] Collinet, B., Herve, M., Pecorari, F., Minard, P., Eder, O. and Desmadril, M. (2000) J. Biol. Chem. 275, 17428–17433.
[5] Futami, J., Tsushima, Y., Murato, Y., Tada, H., Sasaki, J., Seno, M. and Yamada, H. (1997) DNA Cell Biol. 16, 413–419.
[6] Rybak, S.M. and Newton, D.L. (1999) Exp. Cell Res. 253, 325–335.
[7] Futami, J., Maeda, T., Kitazoe, M., Nukui, E., Tada, H., Seno, M., Kosaka, M. and Yamada, H. (2001) Biochemistry 40, 7518–7524.
[8] Leland, P.A., Staniszewski, K.E., Kim, B.M. and Raines, R.T. (2001) J. Biol. Chem. 276, 43095–43102.
[9] Futami, J., Seno, M., Ueda, M., Tada, H. and Yamada, H. (1999) Protein Eng. 12, 1013–1019.
[10] Klink, T.A. and Raines, R.T. (2000) J. Biol. Chem. 275, 17463–17467.
[11] Maeda, T., Mahara, K., Kitazoe, M., Futami, J., Takidani, A., Kosaka, M., Tada, H., Seno, M. and Yamada, H. (2002) J. Biochem. (Tokyo) 132, 737–742.
[12] Futami, J., Tada, H., Seno, M., Ishikami, S. and Yamada, H. (2000) J. Biochem. (Tokyo) 128, 245–250.
[13] Futami, J., Seno, M., Kosaka, M., Tada, H., Seno, S. and Yamada, H. (1995) Biochem. Biophys. Res. Commun. 216, 406–413.
[14] Futami, J., Tsushima, Y., Tada, H., Seno, M. and Yamada, H. (2000) J. Biochem. (Tokyo) 127, 435–441.
[15] Gill, S.C. and von Hippel, P.H. (1989) Anal. Biochem. 182, 319–326.
[16] Futami, J., Nukui, E., Maeda, T., Kosaka, M., Tada, H., Seno, M. and Yamada, H. (2002) J. Biochem. (Tokyo) 132, 223–228.
[17] Tada, H., Shiho, O., Kuroshima, K., Koyama, M. and Tsukamoto, K. (1986) J. Immunol. Methods 93, 157–165.
[18] Suzuki, M., Saxena, S.K., Boix, E., Prill, R.J., Vasandani, V.M., Ladner, J.E., Sung, C. and Youle, R.J. (1999) Nat. Biotechnol. 17, 265–279.
[19] Seno, M., Sasada, R., Kurokawa, T. and Igarashi, K. (1990) Eur. J. Biochem. 188, 239–245.
[20] Kobe, B. and Deisenhofer, J. (1995) Nature 374, 183–186.
[21] Gaur, D., Swaminathan, S. and Batra, J.K. (2001) J. Biol. Chem. 276, 24978–24984.
[22] Minard, P., Scalley-Kim, M., Watters, A. and Baker, D. (2001) Protein Sci. 10, 129–134.
[23] Imoto, T., Yamada, H. and Ueda, T. (1986) J. Mol. Biol. 190, 647–649.
[24] Yamada, H., Ueda, T. and Imoto, T. (1993) J. Biochem. 114, 398–403.
[25] Liuzzo, J.P. and Moscatelli, D. (1996) Blood 87, 245–255.
[26] Springer, B.A., Pantoliano, M.W., Barbera, F.A., Gunyuzlu, P.L., Thompson, L.D., Herblin, W.F., Rosenfeld, S.A. and Book, G.W. (1994) J. Biol. Chem. 269, 26879–26884.
[27] Zhang, J.D., Cousens, L.S., Barr, P.J. and Sprang, S.R. (1991) Proc. Natl. Acad. Sci. USA 88, 3446–3450.
[28] Sayle, R.A. and Milner-White, E.J. (1995) Trends Biochem. Sci. 20, 374.

Activin A and Betacellulin

Effect on Regeneration of Pancreatic β-Cells in Neonatal Streptozotocin-Treated Rats

Lei Li,[1] Zhaohong Yi,[1] Masaharu Seno,[2] and Itaru Kojima[1]

Activin A and betacellulin (BTC) are thought to regulate differentiation of pancreatic β-cells during development and regeneration of β-cells in adults. In the present study, we used neonatal rats treated with streptozotocin (STZ) to investigate the effects of activin A and BTC on regeneration of pancreatic β-cells. One-day-old Sprague-Dawley rats were injected with STZ (85 μg/g) and then administered for 7 days with activin A and/or BTC. Treatment with activin A and BTC significantly reduced the plasma glucose concentration and the plasma glucose response to intraperitoneal glucose loading. The pancreatic insulin content and β-cell mass in rats treated with activin A and BTC were significantly increased compared with the control group on day 8 and at 2 months. Treatment with activin A and BTC significantly increased the DNA synthesis in preexisting β-cells, ductal cells, and δ-cells. The number of islet cell-like clusters (ICCs) and islets was significantly increased by treatment with activin A and BTC. In addition, the number of insulin/somatostatin-positive cells and pancreatic duodenal homeobox-1/somatostatin-positive cells was significantly increased. These results indicate that, in neonatal STZ-treated rats, a combination of activin A and BTC promoted regeneration of pancreatic β-cells and improved glucose metabolism in adults. *Diabetes* 53:608–615, 2004

Diabetes is characterized by absolute or relative deficiency of insulin secretion from pancreatic β-cells, and the β-cell mass is critical in the pathophysiology of diabetes (1,2). Although pancreatic stem cells have not been fully characterized (3), there are several lines of evidence showing that pancreatic stem cells exist in adults and differentiate into β-cells (β-cell neogenesis) in response to an increased demand for insulin (4–7). In pathological conditions, however, β-cell neogenesis is not sufficient to compensate for the needs for insulin. Therefore, investigation of the factors promoting β-cell neogenesis has raised great interest in the past few years (8).

Betacellulin (BTC) belongs to the epidermal growth factor family and is isolated from conditioned medium of insulinoma cells (9). The expression of BTC is predominantly found in the pancreas and the intestine. Specifically, immunoreactive BTC is found in endocrine precursor cells of the fetal pancreas and in insulin-secreting cells of patients with nesidioblastosis (10). Regarding its action, BTC converts amylase-secreting pancreatic AR42J cells into insulin-producing cells (11) and also has a mitogenic effect in human undifferentiated pancreatic epithelial cells (12). These results suggest that BTC plays an important role in regulating growth and/or differentiation of endocrine precursor cells of the pancreas. In this regard, we and others (13–15) have shown that BTC improves glucose metabolism by promoting β-cell regeneration in diabetic animals. Hence, BTC is a potentially intriguing growth factor in treating diabetes.

Activin A, a member of the transforming growth factor-β (TGF-β) superfamily, regulates growth and differentiation of many types of cells (16) and also regulates pancreatic development and endocrine determination (17,18). In vitro, activin A converts AR42J cells into pancreatic polypeptide-producing endocrine cells (11). This is achieved by inducing the expression of neurogenin 3 (19), a critical transcription factor in regulating differentiation of endocrine cells (20,21). Activin A also induces differentiation of human fetal pancreatic endocrine cells (12). Recently, we showed that the expression of activin A was upregulated in the pancreatic duct during pancreatic regeneration (22). Thus, it is possible that activin A regulates neogenesis of β-cells in vivo.

Treatment of neonatal rats with streptozotocin (STZ) provides a useful model for investigating β-cell regeneration (23–26). It has been reported that β-cell regeneration occurs through both increasing the replication of preexisting β-cells and neogenesis from the precursor cells located in or by the pancreatic duct. Because of the limited β-cell regeneration in this model, however, adult rats exhibit decreased β-cell mass and develop type 2 diabetes (27–28). In the present study, using neonatal STZ-treated rats, we investigated the effect of administration of activin A and BTC on β-cell regeneration. The results show that treatment with activin A and BTC during the neonatal

From the [1]Department of Cell Biology, Institute for Molecular and Cellular Regulation, Gunma University, Maebashi, Japan; and the [2]Department of Bioscience and Biotechnology, Graduate School of Natural Science and Technology, Okayama University, Okayama, Japan.

Address correspondence and reprint requests to Itaru Kojima, MD, Institute for Molecular & Cellular Regulation, Gunma University, Maebashi 371-8512, Japan. E-mail: ikojima@showa.gunma-u.ac.jp.

Received for publication 18 August 2003 and accepted in revised form 12 November 2003.

BTC, betacellulin; ICC, islet cell-like cluster; IPGTT, intraperitoneal glucose tolerance test; PDX, pancreatic duodenal homeobox; STZ, streptozotocin; TGF-β, transforming growth factor-β TUNNEL, terminal deoxynucleodidyl transferase.

period improves the glucose metabolism in adults by promoting β-cell regeneration.

RESEARCH DESIGN AND METHODS

Pregnant Sprague-Dawley rats (17 days of pregnancy) were obtained from Japan SLC, Inc. (Shizuoka, Japan). The pregnant rats were caged individually with free access to standard diet and water and were checked at 0900 and 1700 daily for delivery of pups. One-day-old neonates received a single intraperitoneal injection of 85 μg/g body wt of streptozotocin (STZ) (Wako, Japan) freshly dissolved in 0.05 mmol/l citrate buffer (pH 4.5). The number of newborns per litter was kept between 9 and 13. The pups were left with their mothers until 4 weeks old. All neonates were tested 1 day after the STZ treatment (day 1) for blood glucose using Accu-Chek Active (Roche Diagnostics, Heidelberg, Germany). The animals were included in the study only if their blood glucose concentration was between 200 and 350 mg/dl on day 1. Animals whose blood glucose was >350 mg/dl on day 1 developed severe diabetes, and the blood glucose concentrations in these animals were >600 mg/dl on day 2 or 3. The mortality rate of these rats was >50% during the first week after the STZ injection.

Five experimental groups were studied: the normal group, STZ group (STZ-injected rats treated with control buffer), STZ/A group (STZ-injected rats treated with activin A), STZ/B group (STZ-rats treated with BTC), and STZ/A+B group (STZ-injected rats treated with activin A and BTC). One day after the STZ injection, the blood glucose concentration was measured and the animals from various litters were randomly placed in five groups. Then, 200 ng/g body wt of recombinant human BTC in PBS (pH 7.4) and 100 ng/g body wt of recombinant human activin A in 10 mmol/l acetic anhydride containing 0.1% BSA (pH 5.5) (11) or control buffer were subcutaneously injected once a day from day 1 to day 7 according to the experimental groups.

The casual blood glucose concentration and the body weight were measured daily between 1400 and 1600 for the first week and then once a week for up to 8 weeks. The plasma insulin concentration was measured on day 8 and week 8 using an insulin assay kit (Morinaga, Yokohama, Japan) with rat insulin as standard. Blood samples were obtained by decapitation on day 8 and from tail vein on week 8. Six weeks after the STZ treatment, an intraperitoneal glucose tolerance test (IPGTT) (2 g/kg body wt) was done after 14 h of fasting. Blood samples from snipped tails were collected in heparinized hematocrit tubes at different time points and assayed for blood glucose, and the remainder was stored at −20°C for insulin assay. At 8 weeks of age, rats were killed by decapitation. The experimental protocol was approved by the Animal Care Committee of Gunma University.

Tissue processing. On day 4 and day 8, the animals were injected intraperitoneally with 1 ml of bromodeoxyuridine (BrdU) labeling reagent per 100 g body wt (cell proliferation kit; Amersham Pharmacia Biotech, Little Chalfont, U.K.) and decapitated after 3 h. The pancreas was excised, weighed, and divided into two parts. One portion from the splenic segment was fixed in 4% paraformaldehyde/PBS overnight at 4°C and processed for paraffin embedding. Four series from each pancreas was cut at intervals of 100 μm in neonate and 300 μm in adults for immunostaining and histomorphometry. Half pancreas from the other portion was homogenized in cold acid-ethanol, heated for 5 min in 70°C water bath, centrifuged, and the supernatant was stored at −20°C until insulin assay.

Sources of antibodies. Sources of the primary antibodies and the dilutions were as follows: guinea pig anti-porcine insulin, 1:1,000 (a generous gift from Dr. T. Matozaki of Gunma University); rabbit anti-human somatostatin, 1:500 (Dako, Carpinteria, CA); rabbit anti-pancreatic duodenal homeobox-1 (PDX-1) 1:3,000 (14); monoclonal mouse anti-BrdU, 1:100 (Amersham, U.K.); rabbit anti-bovine keratin for wide-spectrum screening (CKwss), 1:1,000 (Dako); and rabbit anti-glucose transporter 2 (GLUT2), 1:50 (Biogenesis Ltd, Poole, U.K.).

Sources of the second antibodies and the dilutions were as follows: goat Alexa Fluor 568 conjugated anti-guinea pig IgG, 1:1,000; goat Alexa Fluor 488 conjugated anti-guinea pig IgG, 1:500; goat Alexa Fluor 568 conjugated anti-mouse IgG, 1:1,000; goat Alexa Fluor 488 conjugated anti-mouse IgG, 1:500; goat Alexa Fluor 568 conjugated anti-rabbit IgG, 1:1,000; and goat Alexa Fluor 488 conjugated anti-rabbit IgG, 1:500 (Molecular Probes, Eugene, OR).

Immunohistochemistry. The sections were deparaffinized and rehydrated, incubated in a microwave oven for BrdU-staining, and digested with protein K (Dako) for CK-staining, washed with PBS, and blocked with DAKO protein block solution. The sections were incubated for 1 h at room temperature with a mixture of primary antibody, washed with PBS, and incubated for 45 min at room temperature with a mixture of the second antibody. The counterstaining was done with 4′,6-diamidio-2-phenylindol-HCl (DAPI) (Boehringer Mannheim, Mannheim, Germany). Finally, the sections were mounted with PermaFluor Aqueous Mounting Medium (IMMUNON Thermo, Shandon, PA). Double staining of PDX-1 and somatostatin was performed as described previously (15).

Measurement of the β-cell mass and size. Quantitative evaluation of the β-cell area was performed on insulin-stained sections using image analysis software (National Institutes of Health image) by means of an AX70 Epifluorescence microscope (Olympus, Tokyo, Japan) equipped with a PXL 1400 cooled-charge-coupled device camera system (Photometrics, Tucson, AZ) operated with IP Lab Spectrum software (Signal Analysis, Vienna, VA). At least 40 random fields (magnification ×200) from one section (three sections from different series per block) were measured for the area of insulin-positive cells and these fields. The ratio of the β-cell area was calculated by dividing the area of all insulin-positive cells in one block by the total area of these fields. The β-cell mass was calculated by multiplying the pancreas weight by the ratio of the β-cell area.

The β-cell size was determined on an insulin-stained section by evaluating the mean cross-sectional area of the individual β-cell. The area of the β-cell in islet was measured as described above, and the number of β-cell nuclei in the islet was counted. Ten islets per animal were measured. The mean cross-sectional area of the individual β-cell was calculated by dividing the total β-cell area in the 10 islets by the number of β-cell nuclei in these islets.

Measurement of replication of β-, δ-, and ductal cells. BrdU/insulin-positive cells were analyzed on BrdU/insulin double-stained sections as a marker of replication of preexisting β-cells. The results were expressed as the percentage of BrdU-positive β-cells. The replication of δ-cells was analyzed by BrdU and somatostatin double-staining. The results were expressed as the percentage of BrdU-positive δ-cells. At least 500 β- and δ-cells were counted per animal, and four animals per group were examined. BrdU/CK-positive cells and CK-positive cells were counted on the BrdU/CKwss double-stained sections. At least 1,000 ductal cells per animal (four animals per group) were analyzed. The results were expressed as the percentage of BrdU-positive ductal cells.

β-Cell neogenesis and the number of islets. To assess the β-cell neogenesis, we quantified the number of islet cell-like clusters (ICCs) (less then five cells across). The number of ICCs and islets was counted in the section stained with anti-insulin antibody, and the area in these sections was measured. The data were shown as the number of ICCs or islets per micrometer squared of the pancreatic area. At least three different sections were analyzed per animal (four animals per group).

β-Cell apoptosis. Apoptotic cells were detected by a terminal deoxynucleodidyl transferase (TUNEL) method using an apoptosis in situ detection kit (Wako Jun-yaku, Tokyo, Japan) (29).

Statistical analysis. Results were expressed as means ± SE. For comparisons between two groups, the unpaired *t* test was used. For multiple comparisons, one-way ANOVA was used. A P value <0.05 was considered statistically significant.

RESULTS

Characteristics of neonatal STZ-treated rats. After STZ treatment, neonatal rats exhibited diabetes. Their blood glucose levels were >250 mg/dl 1 day after the STZ treatment (day 1) and peaked on day 2 with a peak value >350 mg/dl. Thereafter, the blood glucose concentration gradually decreased (Fig. 1*A*). After 6 weeks of age, the blood glucose concentration was slightly but significantly elevated in STZ-treated rats (at 6 weeks of age: normal rat 133.2 ± 3.2 [n = 6] versus STZ rats 152.4 ± 3.5 [n = 11]; $P < 0.005$). The mortality rate caused by STZ in this study was not different from that in normal rats (data not shown).

The plasma insulin concentration at 8 weeks of age and the pancreatic insulin content and the β-cell mass on day 8 and 8 weeks of age in STZ-treated rats were severely reduced compared with those of normal rats ($P < 0.001$) (Tables 1 and 2). However, the β-cell size, body weight, and pancreatic weight of the STZ-treated rats were not different from those of normal rats (Tables 1 and 2).

The IPGTT performed at 6 weeks of age showed that STZ-treated rats developed diabetes. The peak value of the plasma glucose concentration in STZ-treated rats was >350 mg/dl and remained high at 60 min (Fig. 1*B*). The

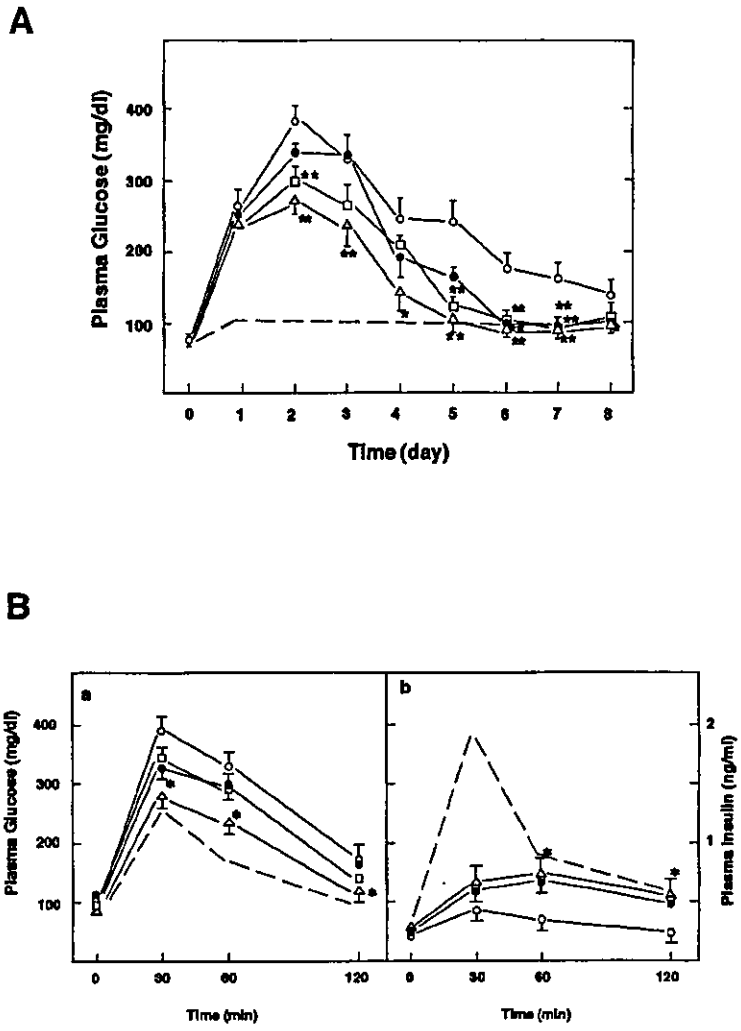

FIG. 1. Changes in the plasma glucose concentration and results of glucose tolerance test in STZ-treated rats. *A*: STZ (85 μg/g) was injected on day 0 (neonate of 1-day-old) and daily injection of activin A and/or BTC was started 1 day later. The plasma glucose concentration was measured. Values are the means ± SE. ○, STZ group (n = 16); ●, STZ/A group (n = 13); □, STZ/B group (n = 13); △, STZ/A+B group (n = 15). —, normal SD rats. *P < 0.05; **P < 0.01 vs. the STZ group. *B*: Glucose tolerance test was performed on 6-week-old rats as described in RESEARCH DESIGN AND METHODS. *a*: Changes in the plasma glucose concentration. *b*: Changes in the plasma insulin concentration. Values are the means ± SE. ○, STZ group (n = 11); ●, STZ/A group (n = 9); □, STZ/B group (n = 9); △, STZ/A+B group (n = 11); —, normal SD rats (n = 6). *P < 0.05 vs. STZ group.

plasma insulin levels in STZ-treated rats were markedly decreased at 30 min compared with those in normal rats (Fig. 1*B*).

The replication of β-cells and ductal cells was determined by insulin/BrdU double immunostaining and CK/BrdU double immunostaining. In STZ-treated rats, the number of insulin/BrdU double-positive cells (STZ-treated 6.5 ± 0.35% vs. normal 4.4 ± 0.15% [n = 4]; P < 0.002) and CK/BrdU double-positive cells (STZ-treated 6.4 ± 0.3% [n = 4] vs. normal 4.1 ± 0.2% [n = 4]; P < 0.001) was significantly increased compared with that of normal rats on day 4.

The islets in STZ-treated rats were smaller than those in normal rats (Fig. 2). In STZ-treated rats, large islets that

TABLE 1
Characteristics of normal, STZ, STZ/A, STZ/B, and STZ/A+B rats on day 8

	Normal	STZ	STZ/A	STZ/B	STZ/A+B
Body weight (g)	14.9 ± 0.6 (10)	13.7 ± 0.8 (16)	14.5 ± 0.7 (13)	14.8 ± 0.6 (14)	13.9 ± 0.7 (15)
Pancreas weight (g)	36.5 ± 1.8 (4)	39.4 ± 1.8 (5)	41 ± 1.0 (9)	39.2 ± 0.5 (5)	44.8 ± 1.8 (4)
Plasma glucose (mg/dl)	114.1 ± 2.6 (6)	153.3 ± 28.4 (16)	123 ± 5.8 (13)	118.8 ± 6.7 (14)	112.6 ± 5.6 (15)
Plasma insulin (ng/ml)	0.386 ± 0.008 (4)	0.342 ± 0.014 (5)	0.380 ± 0.041 (4)	0.360 ± 0.026 (5)	0.435 ± 0.049 (4)
Insulin content					
μg/pancreas	24.6 ± 2.2 (4)	3.46 ± 0.45 (5)	4.45 ± 0.2 (4)	4.48 ± 0.47 (5)	6.06 ± 0.28 (4)*
μg · pancreas	690.2 ± 44.1 (4)	88.3 ± 14.3 (5)	113.8 ± 2.6 (4)	138.0 ± 14.4 (5)†	136.4 ± 7.4 (4)†
β-Cell mass					
mg/pancreas	0.92 ± 0.06 (4)	0.23 ± 0.04 (4)	0.256 ± 0.016 (4)	0.344 ± 0.034 (4)†	0.408 ± 0.046 (4)†
mg/g · pancreas	25.0 ± 1.25 (4)	5.89 ± 0.91 (4)	6.24 ± 0.26 (4)	8.80 ± 1.06 (4)†	9.14 ± 1.06 (4)†
β-Cell size (μm^2)	92.3 ± 4.8 (4)	97.1 ± 6.3 (4)	98.5 ± 4.2 (4)	96.4 ± 3.8 (4)	95.6 ± 5.4 (4)

Data are means ± SE (n). Neonatal rats were treated with STZ and then activin A and/or BTC were administered for 7 days. Various parameters were measured on day 8. Animals were in the nonfasting state. *P < 0.05; †P < 0.01 vs. STZ group.

TABLE 2
Characteristics of normal, STZ, STZ/A, STZ/B, and STZ/A+B rats are 2 months

	Normal	STZ	STZ/A	STZ/B	STZ/A+B
Body weight (g)	236.8 ± 11.6 (6)	225.2 ± 12.5 (11)	236.0 ± 9.7 (9)	238.4 ± 15.1 (9)	228.9 ± 11.7 (11)
Pancreas weight (g)	0.869 ± 0.024 (6)	0.856 ± 0.022 (11)	0.898 ± 0.027 (9)	0.923 ± 0.043 (9)	0.914 ± 0.038 (11)
Plasma glucose (mg/dl)	135.6 ± 4.4 (6)	163.5 ± 4.0 (11)	154 ± 4.8 (9)	151.1 ± 4.1 (9)	148.5 ± 3.4 (11)*
Plasma insulin (ng/ml)	2.40 ± 0.43 (6)	0.94 ± 0.14 (8)	1.10 ± 0.18 (7)	1.138 ± 0.25 (7)	1.02 ± 0.14 (8)
Insulin content					
μg/pancreas	103.3 ± 7.5 (6)	41.2 ± 1.8 (11)	45.8 ± 3.7 (9)	51.6 ± 4.0 (9)*	64.8 ± 2.1 (11)†
μg/g · pancreas	118.8 ± 8.1 (6)	46.9 ± 2.8 (11)	51.1 ± 4.1 (9)	56.1 ± 4.4 (9)	60.0 ± 3.5 (11)†
β-Cell mass					
mg/pancreas	8.11 ± 0.81 (4)	2.87 ± 0.31 (4)	3.55 ± 0.36 (4)	4.53 ± 0.41 (4)*	5.89 ± 0.35 (4)†
mg/g · pancreas	9.67 ± 0.86 (4)	3.37 ± 0.31 (4)	3.85 ± 0.28 (4)	4.87 ± 0.29 (4)*	5.93 ± 0.33 (4)*
β-Cell size (μm^2)	192.6 ± 4.5 (4)	202.2 ± 5.6 (4)	199.6 ± 3.5 (4)	195.3 ± 2.7 (4)	197.7 ± 3.8 (4)

Data are means ± SE (n). Neonatal rats were treated with STZ and then activin A and/or BTC were administered for 7 days. Various parameters were measured 2 months later. Animals were in the nonfasting state. *$P < 0.05$; †$P < 0.01$ vs. STZ group.

are usually observed in normal rats were absent. Insulin immunoreactivity was weak in β-cells of the islets of the STZ-treated rats. No difference in GLUT2-staining of β-cells was observed between normal and STZ-treated rats (Fig. 2).

Effect of BTC and activin A on blood glucose and IPGTT. Treatment with a combination of activin A and BTC significantly decreased the blood glucose in neonatal STZ-rats at the early time points (Fig. 1*A*). The effect of activin A and BTC was persistent until adult age (Table 2). The body weight, pancreatic weight, β-cell size, and plasma insulin concentration were not changed by either of the treatments (Tables 1 and 2).

A glucose tolerance test was performed at 6 weeks of age to assess the long-term effect of activin A and BTC. Compared with the STZ groups, the blood glucose in the STZ/A+B group was significantly lower after 30, 60, and 120 min, although the plasma insulin concentration was not significantly increased compared with those in the STZ group (Fig. 1*B*). There was no significant difference in glucose tolerance between the STZ/A or STZ/B group and STZ group.

Effect of BTC and activin A on the insulin content and the β-cell mass. Treatment with activin A and BTC improved the glucose metabolism and IPGTT. We then examined the pancreatic insulin content and the β-cell mass in the experimental groups on day 8 and at 2 months of age. The results are shown in Tables 1 and 2. The pancreatic insulin content in the STZ/A+B group increased 70% at 8 days of age and >30% at 2 months of age compared with that in the STZ group ($P < 0.01$) (Tables 1 and 2). Similarly, the β-cell mass also significantly increased 77% on day 8 and 69% at 2 months of age in the STZ/A+B group ($P < 0.05$). The treatment with activin A and BTC did not change the β-cell size (Table 2). The pancreatic insulin content and the β-cell mass in STZ/B group were also significantly increased ($P < 0.05$). On the other hand, the pancreatic insulin content and the β-cell mass in the STZ/A group was not significantly changed compared with that of the STZ group.

Effect of BTC and activin A on the regeneration of β-cells. The above results showed that treatment with activin A and BTC increased the β-cell mass without affecting the β-cell size. These factors thus increased the number of β-cells. The β-cell number is determined by a balance between the generation of β-cells and β-cell death. When we assessed apoptosis by TUNEL method, the frequency of apoptotic β-cells was very low (data not shown). We therefore investigated the effect of BTC and activin A on the regeneration of β-cells in STZ-treated neonatal rats.

There are at least three pathways for β-cell regeneration: replication of preexisting β-cells, neogenesis from the precursors located in the duct, and transdifferentiation of non–β-cells in islets. In the STZ-treated group, replications of β-cells were significantly higher than those in normal rats. The treatment with A+B or BTC alone significantly increased the replication of β-cells (Fig. 3). Though it is difficult to estimate the neogenesis of β-cells from ductal cells, treatment with activin A and BTC or BTC alone significantly increased the proliferation of ductal cells and the number of ICCs compared with STZ group rats (Fig. 4). The number of islets in STZ/A+B and STZ/B significantly increased, although there was no difference between STZ and normal rats (Fig. 4*D*).

It was shown that β-cell regeneration occurred in adult STZ-treated mice through transdifferentiation of δ-cells to β-cells (6,30). We then examined whether regeneration

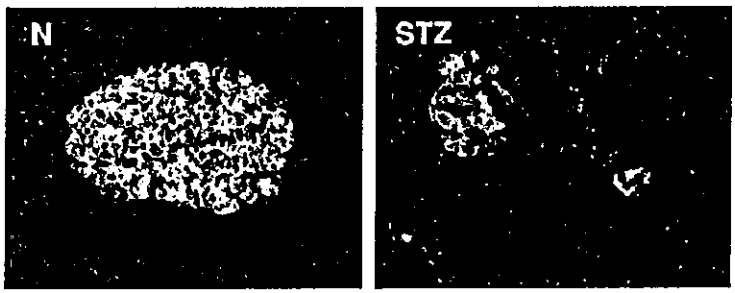

FIG. 2. Morphology of typical islets in normal and STZ-treated rats. Pancreatic sections obtained from neonatal STZ-treated (STZ) and nontreated (N) rats at 2 months of age were stained with anti-insulin (red) and anti-GLUT2 antibodies (green). Nuclei were stained with DAPI (blue) (original magnification ×200).

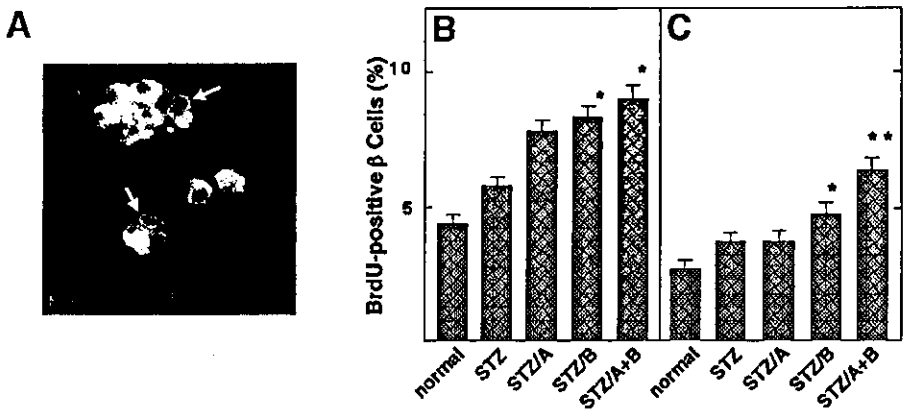

FIG. 3. Effects of activin A and BTC on the replication of insulin-positive cells in STZ-treated neonatal rats. *A*: Double immunostaining for insulin (green) and BrdU (red) in STZ/A+B rats on day 4 (original magnification ×400). The arrows show cells positive for insulin and BrdU. *B*: Effects of activin A and BTC on day 4. The numbers of BrdU/insulin-positive cells and insulin positive-cells were measured. The results were expressed as the percent of BrdU-positive β-cell. Values are the mean ± SE ($n = 4$). *C*: Effect of activin A and BTC on day 8. Values are the means ± SE ($n = 4$). *$P < 0.05$; **$P < 0.01$ vs. the STZ group.

through this route occurred in STZ-treated neonatal rats. We investigated the changes in δ-cells in STZ-treated neonatal rats. Replication of δ-cells was significantly increased compared with that of normal rats on day 4 (STZ-treated 4.4 ± 0.4% vs. normal 2.8 ± 0.3% [$n = 4$]; $P < 0.02$). Treatment with activin A and BTC or BTC alone further promoted the replication of δ-cells (Fig. 5*B*). In addition, the number of PDX-1/somatostatin double-positive cells was markedly increased in STZ-treated neonatal rats (STZ-treated 35.2 ± 3.2% vs. normal 26.9 ± 2.1% [$n = 4$]; $P < 0.05$). Treatment with activin A and BTC or BTC alone further increased the number of PDX-1/somatostatin double-positive cells compared with STZ group rats (Fig. 6*B*). In STZ-treated rats, insulin/somatostatin double-positive cells were observed (Fig. 6*D*). The number of insulin/somatostatin double-positive cells was significantly increased in rats treated with activin A and BTC (Fig. 6*E*).

DISCUSSION

Newborn rats treated with STZ at birth have been widely used to study the regeneration of pancreatic β-cells (23–26). In the present study, we used this model to investigate the effect of activin A and BTC on regeneration of pancreatic β-cells. We injected activin A subcutaneously at a daily dose of 100 ng/g for 7 days. This dose of activin A was shown to promote bone formation in rats (31). At this dose, activin A slightly decreased the plasma glucose concentration on days 6 and 7, but the effect was minimal. Higher doses may have been more effective but we could not examine the possibility because of the limited amount of activin A available. Nevertheless, activin A significantly enhanced the effect of BTC on both glucose metabolism and β-cell regeneration. For example, activin A augmented the BTC effect on the insulin content on day 8 and week 8. Also, a combination of activin A and BTC but not BTC alone increased the number of BrdU-positive ductal cells at day 4 and the number of insulin/somatostatin double-positive cells. As in AR42J cells (11), activin A and BTC thus acted coordinately and induced regeneration of β-cells. As in the case with glucagon-like peptide-1 and its long-acting agonist exendin (26), a combination of activin A and BTC is effective in improving diabetes in neonatal STZ-treated rats.

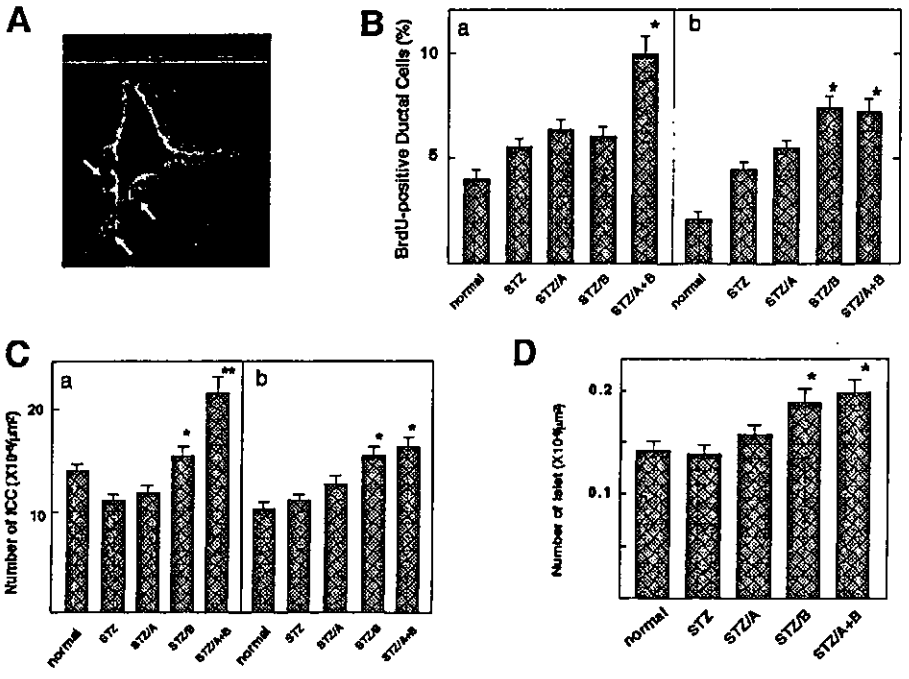

FIG. 4. Effects of activin A and BTC on replication of ductal cells and the number of ICCs and islets. *A*: Double immunostaining for CK (green) and BrdU (red) in STZ/A+B rats on day 4 (original magnification ×400). Nuclei were stained by DAPI. Arrows show the cells positive for CK and BrdU. *B*: Effect of activin A and BTC on replication of ductal cells on day 4 (*a*) and day 8 (*b*). The numbers of BrdU/insulin-positive cells and CK-positive cells were counted. The results were expressed as the percent of BrdU-positive duct cells. Values are the means ± SE ($n = 4$). *$P < 0.05$ vs. the STZ group. *C*: Effect of activin A and BTC on the number of ICCs. *a*: Effect of activin A and BTC on the number of ICCs on day 4. *b*: Effect of activin A and BTC on the number of ICCs on day 8. Data were shown as the number of ICCs per micrometer squared of the pancreatic area. Values are the means ± SE ($n = 4$). *$P < 0.05$; **$P < 0.01$ vs. the STZ group. *D*: The number of islets was counted in the section stained with insulin in 2-month-old rats. Data were expressed as the number of islets per micrometer squared of the pancreatic area. Values are the means ± SE ($n = 4$). *$P < 0.05$ vs. the STZ group.

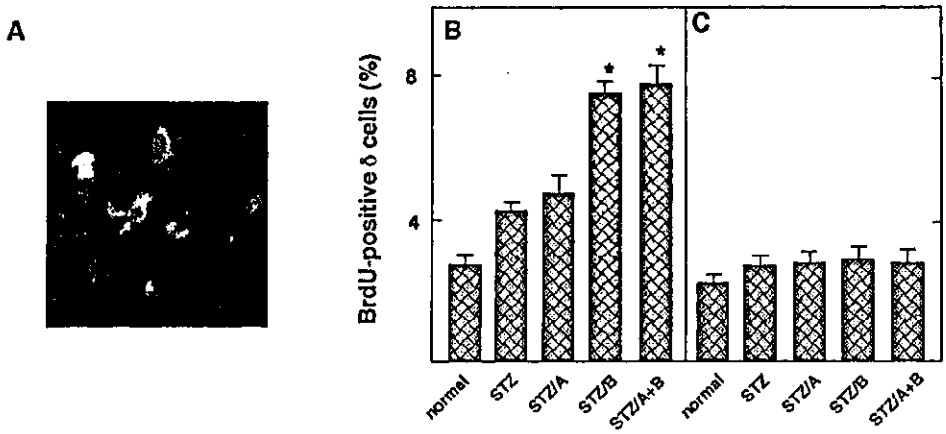

FIG. 5. Effects of activin A and BTC on replication of δ-cells. *A*: Double immunostaining for somatostatin (green) and BrdU (red) in STZ/A+B rats on day 4 (original magnification ×400). Nuclei were stained with DAPI (blue). *B*: Effect of activin A and BTC on the replication of δ-cells on day 4. BrdU/somatostatin-positive cells and somatostatin-positive cells were counted on day 4. The results were shown as the percent of BrdU-positive δ-cells. *C*: Effect of activin A and BTC on the replication of δ-cell on day 8. Values are the means ± SE (n = 4). *P < 0.05 vs. the STZ group.

In this study, we observed that treatment with activin A and BTC was effective in improving glucose metabolism in newborn rats treated with STZ. Although we could not quantify the route by which these factors promoted β-cell regeneration, the treatment increased the β-cell mass and the insulin content (Tables 1 and 2). As shown in Fig. 3, treatment with activin A and BTC promoted replication of preexisting β-cells. In addition, replication of ductal cells and the number of ICCs were increased by treatment with activin A and BTC (Fig. 4). Consistent with these data, the number of islets in the STZ/A+B group was increased. Collectively, treatment with activin A and BTC also promoted neogenesis from precursor cells located in the pancreatic duct. These data are in accordance with the previous report on the effect of BTC on β-cell regeneration (13–15).

There was no significant increase in the number of ICCs on days 4 and 8 in rats treated with STZ compared with that of normal rats (Fig. 4*C*). In agreement with this finding, the number of islets in 2-month-old rats treated with STZ was the same as that in normal rats of the same age (Fig. 4*D*). A similar result was previously reported by other research groups (28,32). These results suggest that neogenesis from the precursor cells located in or by the pancreatic duct in this model may not be accelerated compared with that in normal rats. Based on the data on the β-cell size and β-cell replication on days 4 and 8, we estimated the increase in the β-cell mass from day 4 to day 8 using the previously described method for evaluating the parameter of β-cell growth (32,33). In normal rats, we found that the predicted increase in β-cell mass through β-cell replication was 64%, which is slightly higher than the increase in the measured β-cell mass (52%) during this period. Of course, the neogenesis from the duct precursor may also contribute to the in crease in the β-cell mass. There is a discrepancy between the measured β-cell mass and predicted β-cell mass. In fact, β-cell apoptosis may participate in the remodeling of the endocrine pancreas in neonatal rats (38), although the frequency of apoptosis β-cell was low in the present study. In STZ-treated neona-

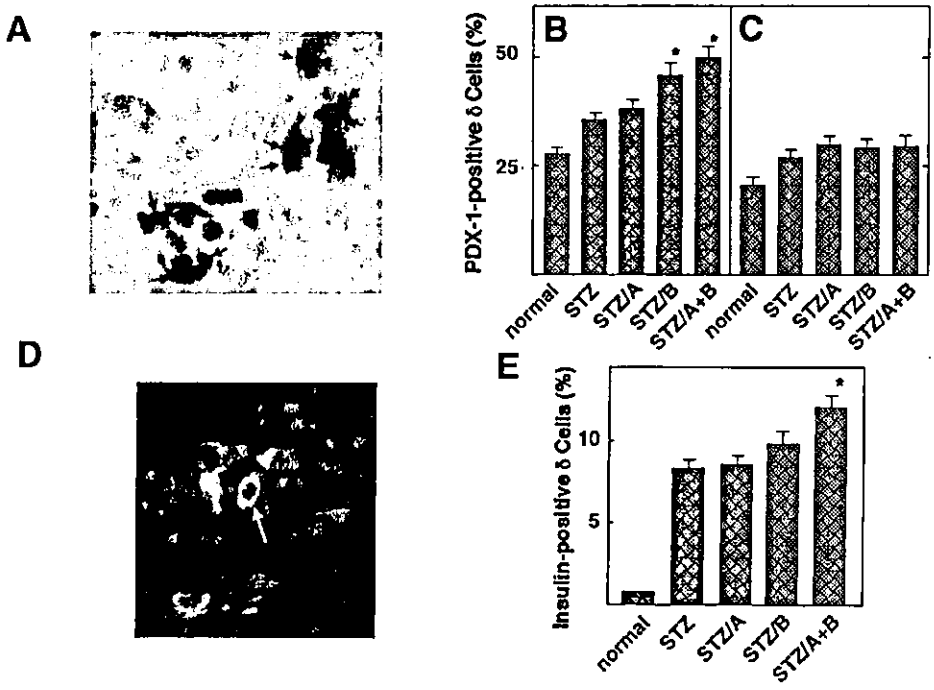

FIG. 6. Effect of activin A and BTC on the number of PDX-1–positive δ-cells and insulin/somatostatin double-positive cells. *A*: Double immunostaining for somatostatin (red) and PDX-1 (brown) in STZ/A+B rats on day 4. Nuclei were stained with hematoxylin (blue). PDX-1/somatostatin double-positive cells were indicated by the arrow. *B*: Effect of activin A and BTC on the number of PDX-1–positive δ-cells on day 4. PDX-1/somatostatin-positive cells and somatostatin-positive cells were counted. The data were shown as the percent of PDX-1–positive δ-cells. *C*: Effect of activin A and BTC on the number of PDX-1–positive δ-cells on day 8. Values are the means ± SE (n = 4). *P < 0.05 vs. the STZ group. *D*: Double-staining for insulin (red) and somatostatin (green) in STZ/A+B rats on day 4. Nuclei were stained with DAPI (blue). The arrow shows a cell expressing both insulin and somatostatin. *E*: Changes in the number of insulin/somatostatin double-positive cells were counted. Values are the means ± SE (n = 4). *P < 0.05 vs. the STZ group.

tal rats, the increase in the measured β-cell mass was 259%, while the increase in the predicted β-cell mass through β-cell replication was 98%. Therefore, replication of preexisting β-cells cannot explain the drastic increase in the β-cell mass during the early time point in STZ-treated neonatal rats. Another possible pathway is thought to exist to increase the β-cell mass in this regeneration model. Recently, studies have shown that β-cell regeneration has an alternate route, namely differentiation of precursor cells located in islets (6,30). Also, islet neogenesis from intraislet precursor cells of the diabetic pancreas has been reported (34). It is therefore necessary to investigate whether β-cell neogenesis from the precursor cells located in the islets occurs in neonatal STZ-treated rats. In STZ-treated neonatal rats, temporal increases in the replication of δ-cells (day 4: 4.4 ± 0.4%, day 8: 2.6 ± 0.15% [n = 4]) and the number of PDX-1/somatostatin cells (day 4: 35.2 ± 1.6%, day 8: 28.7 ± 1.7% [n = 4]) were observed, and many somatostatin/insulin double-positive cells that rarely exist in normal rats appeared on day 4 (Fig. 6). PDX-1/somatostatin cells and insulin/somatostatin cells are presumptive β-cell precursors in STZ-treated mice and pancreatic development (6,30,35). Consequently, neogenesis from the precursor cells located in the islets at least partly contributed to the increase in the β-cell mass in this model. As shown in Figs. 5 and 6, administration of activin A and BTC significantly increased the number of BrdU/somatostatin-, PDX-1/somatostatin-, and insulin/somatostatin-positive cells. It is therefore likely that BTC and activin A promoted β-cell neogenesis from precursor cells located in the islets.

The treatment with activin A and BTC significantly increased the β-cell mass and the insulin content and decreased the plasma glucose concentration. Also, the plasma glucose response after glucose loading was significantly improved. However, rapid insulin response to glucose loading was still absent. The reason for the improved glucose response in the absence of rapid insulin secretion is not totally clear. One possible reason is that small increases in insulin secretion, albeit delayed, may be beneficial for whole-body glucose metabolism and thus improve glucose tolerance. Although the insulin content and the β-cell mass was increased by activin A and BTC, the insulin response was delayed. Similar results were previously reported by other research groups as well (26,28,36). The reason that the insulin-secreting ability of regenerating β-cell is low in response to glucose loading is still not totally clear. One possible reason is that the β-cell mass was not restored because at least 75% of the normal β-cell mass is needed for maintaining normal glucose homeostasis (37). Another possible reason is that, in STZ-treated rats, there were no large islets that usually exist in normal rats (Fig. 2). It is possible that large islets may play an important role in insulin release in response to glucose loading. The treatment with activin A and BTC partly increased the size of islets, but the largest islets in STZ/A+B adult rats could not be comparable to that of normal rats of the same age. It is also possible that the glucose-sensing mechanism is impaired in regenerating β-cells (28). This is partly due to glucotoxicity during neonatal period.

In summary, in STZ-treated neonatal rats, treatment with activin A and BTC coordinately promoted regeneration of β-cells, increased the β-cell mass and insulin content, and persistently improved glucose metabolism in adult age. The β-cell neogenesis from the precursor cells located in the islets may play an important role during the early phase of pancreatic regeneration in neonatal rats treated with STZ.

ACKNOWLEDGMENTS

This study was supported by Grant-in Aid for the Project for Realization of Regenerative Medicine, Scientific Research from the Ministry of Education, Science, Sports and Culture of Japan. L.L. is a postdoctoral research fellow supported by the Japanese Society for the Promotion of Science.

We thank Mayumi Odagiri for secretarial assistance.

REFERENCES

1. Kloppel G, Lohr M, Habich K, Oberholzer M, Heitz PU: Islet pathology and the pathogenesis of type 1 and type 2 diabetes mellitus revisited. *Surv Synth Pathol Res* 4:110–125, 1985
2. Weir GC, Bonner-Weir S, Leahy JL: Islet mass and function in diabetes and transplantation. *Diabetes* 39:401–405, 1990
3. Bonner-Weir S, Sharma A: Pancreatic stem cells. *J Pathol* 197:519–526, 2002
4. Bonner-Weir S, Baxter LA, Schuppin GT, Smith FE: A second pathway for regeneration of adult exocrine and endocrine pancreas: a possible recapitulation of embryonic development. *Diabetes* 42:1715–1720, 1993
5. Wang RN, Kloppel G, Bouwens L: Duct- to islet-cell differentiation and islet growth in the pancreas of duct-ligated adult rats. *Diabetologia* 38:1405–1411, 1995
6. Guz Y, Nasir I, Teitelman G: Regeneration of pancreatic beta cells from intra-islet precursor cells in an experimental model of diabetes. *Endocrinology* 142:4956–4968, 2001
7. Gu D, Lee MS, Krahl T, Sarvetnick N: Transitional cells in the regenerating pancreas. *Development* 120:1873–1881, 1994
8. Nielsen JH, Svensson C, Galsgaard ED, Moldrup A, Billestrup N: Beta cell proliferation and growth factors. *J Mol Med* 77:62–66, 1999
9. Shing Y, Christofori G, Hanahan D, Ono Y, Sasada R, Igarashi K, Folkman J: Betacellulin: a mitogen from pancreatic beta cell tumors. *Science* 259:1604–1607, 1993
10. Miyagawa J, Hanafusa O, Sasada R, Yamamoto K, Igarashi K, Yamamori K, Seno M, Tada H, Namino T, Li M, Yamagata K, Nakajima H, Namba M, Kuwajima M, Matsuzawa Y: Immunohistochemical localization of betacellulin, a new member of the EGF family, in normal human pancreas and islet tumor cells. *Endocr J* 6:755–764, 1999
11. Mashima H, Ohnishi H, Wakabayashi K, Mine T, Miyagawa J, Hanafusa T, Seno M, Yamada H, Kojima I: Betacellulin and activin A coordinately convert amylase-secreting pancreatic AR42J cells into insulin-secreting cells. *J Clin Invest* 97:1647–1654, 1996
12. Demeterco C, Beattie GM, Dib SA, Lopez AD, Hayek A: A role for activin A and betacellulin in human fetal pancreatic cell differentiation and growth. *J Clin Endocrinol Metab* 85:3892–3897, 2000
13. Yamamoto K, Miyagawa J, Waguri M, Sasada R, Igarashi K, Li M, Nammo T, Moriwaki M, Imagawa A, Yamagata K, Nakajima H, Namba M, Tochino Y, Hanafusa T, Matsuzawa Y: Recombinant human betacellulin promotes the neogenesis of beta-cells and ameliorates glucose intolerance in mice with diabetes induced by selective alloxan perfusion. *Diabetes* 49:2021–2027, 2000
14. Li L, Seno M, Yamada H, Kojima I: Promotion of beta-cell regeneration by betacellulin in ninety percent-pancreatectomized rats. *Endocrinology* 142:5379–5385, 2001
15. Li L, Seno M, Yamada H, Kojima I: Betacellulin improves glucose metabolism by promoting conversion of intraislet precursor cells to β-cells in streptozotocin-treated mice. *Am J Physiol* 285:E577–E583, 2003
16. Massague J, Chen YG: Controlling TGF-beta signaling. *Genes Dev* 14:627–644, 2000
17. Kim SK, Hebrok M, Li E, Oh SP, Schrewe H, Harmon EB, Lee JS, Melton DA: Activin receptor patterning of foregut organogenesis. *Genes Dev* 14:1866–1871, 2000
18. Yamaoka T, Idehara C, Yano M, Matsushita T, Yamada T, Ii S, Moritani M, Hata J, Sugino H, Noji S, Itakura M: Hypoplasia of pancreatic islets in

transgenic mice expressing activin receptor mutants. *J Clin Invest* 102: 294–301, 1998
19. Zhang YQ, Mashima H, Kojima I: Changes in the expression of transcription factors in pancreatic AR42J cells during differentiation into insulin-producing cells. *Diabetes* 50:S10–S14, 2001
20. Apelqvist A, Li H, Sommer L, Beatus P, Anderson DJ, Honjo T, Hrabe de Angelis M, Lendahl U, Edlund H: Notch signalling controls pancreatic cell differentiation. *Nature* 400:877–881, 1999
21. Gradwohl G, Dierich A, LeMeur M, Guillemot F: Neurogenin3 is required for the development of the four endocrine cell lineages of the pancreas. *Proc Natl Acad Sci U S A* 97:1607–1611, 2000
22. Zhang YQ, Zhang H, Maeshima A, Kurihara H, Miyagawa J, Takeuchi T, Kojima I: Up-regulation of the expression of activins in the pancreatic duct by reduction of the beta-cell mass. *Endocrinology* 143:3540–3547, 2002
23. Cantenys D, Portha B, Dutrillaux MC, Hollande E, Roze C, Picon L: Histogenesis of the endocrine pancreas in newborn rats after destruction by streptozotocin: an immunocytochemical study. *Virch Arch* 35:109–122, 1981
24. Dutrillaux MC, Portha B, Roze C, Hollande E: Ultrastructural study of pancreatic B cell regeneration in newborn rats after destruction by streptozotocin. *Virch Arch* 39:173–185, 1982
25. Wang RN, Bouwens L, Kloppel G: Beta-cell proliferation in normal and streptozotocin-treated newborn rats: site, dynamics and capacity. *Diabetologia* 37:1088–1096, 1994
26. Tourrel C, Bailbe D, Meile MJ, Kergoat M, Portha B: Glucagon-like peptide-1 and exendin-4 stimulate beta-cell neogenesis in streptozotocin-treated newborn rats resulting in persistently improved glucose homeostasis at adult age. *Diabetes* 50:1562–1570, 2001
27. Portha B, Levacher C, Picon L, Rosselin G: Diabetogenic effect of streptozotocin in the rat during the perinatal period. *Diabetes* 23:889–895, 1974
28. Bonner-Weir S, Trent DF, Honey RN, Weir GC: Responses of neonatal rat islets to streptozotocin: limited B-cell regeneration and hyperglycemia. *Diabetes* 30:64–69, 1981
29. Gavrieli Y, Sherman Y, Ben-Sasson SA: Identification of programmed cell death in situ via specific labeling of nuclear DNA fragmentation. *J Cell Biol* 119:493–501, 1992
30. Fernandes A, King LC, Guz Y, Stein R, Wright CV, Teitelman G: Differentiation of new insulin-producing cells is induced by injury in adult pancreatic islets. *Endocrinology* 138:1750–1762, 1997
31. Sakai R, Fujita S, Horie T, Ohyama T, Miwa K, Maki T, Okimoto N, Nakamura T, Eto Y: Activin increases bone mass and mechanical strength of lumbar vertebrae in aged ovariectomized rats. *Bone* 27:91–96, 2000
32. Garofano A, Czernichow P, Breant B: Impaired beta-cell regeneration in perinatally malnourished rats: a study with STZ. *FASEB J* 14:2611–2617, 2000
33. Movassat J, Saulnier C, Portha B: Insulin administration enhances growth of the beta-cell mass in streptozotocin-treated newborn rats. *Diabetes* 46:1445–1452, 1997
34. Banerjee M, Bhonde RR: Islet generation from intra islet precursor cells of diabetic pancreas: in vitro studies depicting in vivo differentiation. *J Pancreas* 4:137–145, 2003
35. Guz Y, Montminy MR, Stein R, Leonard J, Gamer LW, Wright CV, Teitelman G: Expression of murine STF-1, a putative insulin gene transcription factor, in beta cells of pancreas, duodenal epithelium and pancreatic exocrine and endocrine progenitors during ontogeny. *Development* 121:11–18, 1995
36. Blondel O, Bailbe D, Portha B: Relation of insulin deficiency to impaired insulin action in NIDDM adult rats given streptozocin as neonates. *Diabetes* 38:610–617, 1989
37. Turner RC, Holman RR, Matthews D, Hockaday TD, Peto J: Insulin deficiency and insulin resistance interaction in diabetes: estimation of their relative contribution by feedback analysis from basal plasma insulin and glucose concentrations. *Metabolism* 28:1086–1096, 1979
38. Scaglia L, Cahill CJ, Finegood DT, Bonner-Weir S: Apoptosis participates in the remodeling of the endocrine pancreas in the neonatal rat. *Endocrinology* 138:1736–1741, 1997

The Influence of Platelets on the Promotion of Invasion by Tumor Cells and Inhibition by Antiplatelet Agents

Keiichi Suzuki, MD, Koichi Aiura, MD, Masakazu Ueda, MD, and Masaki Kitajima, MD

Objective: Using a chemoinvasion assay, we show that platelets promote invasiveness of 5 pancreatic adenocarcinoma cell lines.

Methods: Gelatin zymography and Western blot analysis were performed to detect metalloproteinase-9 (MMP-9) secreted from tumor cells in the presence or absence of platelets. The effects of antiplatelet agents on the invasiveness of tumor cells and the secretion level of MMP-9 were evaluated.

Results: The number of traversed tumor cells significantly increased when incubated with platelets compared without platelets in all cell lines. The MMP-9 band was detected in all tumor cell lines, and the intensity was obviously greater in conditions of incubation with platelets than without. In the experiment of antiplatelet agents effects, it was confirmed that invasiveness of tumor cells significantly decreased following incubation with cilostazol depending on the concentration in spite of the presence of platelets. The level of MMP-9 also significantly decreased in the ELISA analysis.

Conclusions: These data mean platelets activate invasiveness of tumor cells because of enhanced MMP-9 secretion. Furthermore, antiplatelet drugs may inhibit invasiveness of tumor cells due to decreased MMP-9 secretion, and this inhibition may lead to the suppression of tumor cell invasion. We propose that antiplatelet agents are applicable in clinical treatment to inhibit metastasis of malignant tumor cells.

Key Words: metastasis, matrix metalloproteinase-9, pancreatic cancer, chemoinvasion, zymography

(*Pancreas* 2004;29:132–140)

Pancreatic cancer is the fourth leading cause of cancer death in the United States, with a mortality rate that virtually equals its incidence rate.[1] Despite recent advances in imaging techniques, many pancreatic cancers are still at an advanced stage at the time of diagnosis. Even after radical resection, the overall median survival time of patients with pancreatic adenocarcinoma is only 18 to 20 months, and their overall 5-year survival rate is approximately 10%.[2] Although many researchers have applied various strategies to overcome these problems, no satisfactory results have been obtained.

The interaction between tumor cells and platelets has been attracting attention. This correlation between platelets and tumor cells has also been studied in clinical research. It has been recently reported that the prognosis was poor in patients with cancers of the lung and uterine cervix in whom the preoperative platelet count increased.[3–5] Therefore, we investigated the correlation between platelets and cancer cells in pancreatic adenocarcinoma.

The importance of the interaction between platelets and tumor cells was first recognized by Gasic et al,[6] and thus far various investigations have been performed to examine this interaction. Numerous studies have shown that tumor cells in vitro can induce platelet aggregation, and this ability to aggregate platelets correlated with their ability to cause metastasis in vivo.[7–9]

Platelets were activated and aggregated by ADP produced by tumor cells themselves or released by platelets in contact with tumor cells.[10] Activated platelets secrete adherent proteins, such as fibrinogen, fibronectin, factors V and VIII, and thrombospondin, and strengthen the adherence between tumor cells and platelets or tumor cells and endothelial cells. A morphologic study was performed in which aggregated platelets contacted tumor cells directly and surrounded them.[11] Platelet activation by tumor cells is thought to protect tumor cells from immune surveillance, to enhance tumor cell adhesion to the vascular endothelium, the first step of extravasation, and to provide permeability that would facilitate extravasation and development of tumor metastasis.[12,13] It has been reported that the distant metastasis rate is high in tumor cells that strongly aggregate platelets, while the metastasis rate is low in tumor cells that weakly aggregate platelets, suggesting that the platelet aggregation activity of tumor cells is correlated with the metastasis rate.[14] The distant metastasis rate of tumor cells has been reported to decrease in a laboratory animal model for thrombocytopenia.[15] Moreover, it has been reported that the metastasis rate decreased following administration of prostacyclin (PGI_2), which inhibits platelets.[16] The above-men-

Received for publication October 17, 2003; accepted January 23, 2004.

From the Department of Surgery, Keio University School of Medicine, Tokyo, Japan.

This work was supported by a Grant-in-Aid from the Ministry of Education, Culture, Sports, Science and Technology and a national Grant-in-Aid for encouragement of young scientists.

Reprints: Masakazu Ueda, MD, Department of Surgery, Keio University School of Medicine, 35 Shinanomachi, Shinjuku-ku, Tokyo 160-8582, Japan (e-mail: m_ueda@sc.itc.keio.ac.jp).

tioned findings suggest that platelets may play an important role in promotion of tumor cell invasion.

Since the initial documentation by Liotta and Stetler-Stevenson,[17] a number of reports have focused on and demonstrated the relationship between the extracellular matrix (ECM) and tumor cell invasion and metastasis. The ECM, which is comprised of various types of collagens, fibronectin, elastin, and proteoglycan, is degraded by proteinases such as matrix metalloproteinases (MMPs).[18,19] MMPs are secreted from cancer cells and/or adjacent stromal cells in a latent form and then converted into an active form.[20,21] Therefore, it is recognized that MMPs play an important role in tumor invasion and metastasis. It has been reported that the active form of MMP-2 was detected in samples of pancreatic carcinoma.[22] Recently, it has also been reported that platelets greatly stimulated the secretion of MMP-9 by human mammary tumor cells, leading to an increased invasiveness of these cells in an in vitro invasion model.[23,24]

As described above, many investigations have been performed using various approaches to evaluate the interaction between platelets and tumor cells. However, the precise mechanism of this interaction was and still is unclear, and the effect of antiplatelet agents on this promotion of tumor cell invasiveness has not been investigated in detail.

Therefore, in this study, we investigated whether the presence of platelets can promote the invasiveness of tumor cells and whether platelets can increase the secretion level of MMP-9 from tumor cells in human pancreatic cancer cell lines. Moreover, we evaluated the effect of antiplatelet agents on the levels of invasiveness and on the secretion of MMP-9 from tumor cells by inhibiting platelets to assess the utility of this approach in clinical treatment.

MATERIALS AND METHODS

Reagents

ADP was purchased from MC Medical (Tokyo, Japan). RPMI-1640 medium, bovine serum albumin (BSA), prostaglandin E_1 (PGE_1), hirudin, thrombin, prostacyclin (PGI_2), and eicosapentaenoic acid (EPA) were from Sigma Chemical Co. (St. Louis, MO). R-PE-conjugated mouse antihuman monoclonal antibody against CD62P was from Pharmingen International (San Diego, CA). BioCoat Cell Culture Inserts, Falcon companion Plates, Matrigel Basement Membrane Matrix, and human fibronectin were from Becton Dickinson Labware (Bedford, MA). The Diff-Quick stain kit was from IMEB Inc. (Chicago, IL). The gelatin zymography electrophoresis kit was from Yagai Ltd. (Yamagata, Japan). Multigel was from Daiichi Pure Chemicals Co., Ltd. (Tokyo, Japan) for SDS-PAGE. Antihuman MMP-9 and purified IgG were from Tomiyama Pure Chemical Industries, Ltd. (Tokyo, Japan). Hybond ECL Nitrocellulose membrane, ECL Western blotting system, antimouse IgG antibody, purified human MMP-9, streptavidin/horseradish peroxidase conjugate, and the Biotrak MMP-9 human ELISA system were obtained from Amersham Pharmacia Biotech (Piscataway, NJ). The antiplatelet agent Cilostazol was kindly provided by Otsuka Pharmaceutical Co., Ltd. (Tokyo, Japan). Other reagents were of chemical grade.

Cell Lines

Five human cell lines of adenocarcinoma of the pancreas were prepared, SW.1990, SU 86.86., Capan-2, BxPC-3, and AsPC-1. All of these cell lines were purchased from American Type Culture Collection (Manassas, VA). These cell lines were cultured in RPMI 1640 containing 10% FBS. They were maintained under an atmosphere of 5% CO_2 at 37°C.

Platelet Preparation

In all these examinations, venous blood was collected from the same healthy volunteer. Platelets were isolated in the presence of 0.1 vol of anticoagulant citric acid (0.04 mol/L citric acid, 0.075 mol/L trisodium citrate, 0.14 mol/L glucose, pH 4.5) as described by Aiura et al.[25] Plasma-rich platelets (PRP) were prepared by centrifugation at 200*g* for 15 minutes at room temperature. Washed platelets were prepared by adding 10% anticoagulant citric acid and 2 μL of 50 μg/mL PGE_1 to PRP and were centrifuged at 700*g* for 6 minutes at room temperature. Platelet pellets after removing supernatant were collected and washed by the addition of 9 mL of Tris-NaCl glucose buffer (0.15 mol/L NaCl, 0.05 mol/L Tris HCl, 5 mmol/L glucose), 1 mL of citric acid, and 8 μL of 50 μg/mL PGE_1. The twice-washed platelets were finally suspended in TC medium (RPMI 1640, 0.1% BSA, 10 mmol/L $CaCl_2$, 5 mmol/L $MgCl_2$, 100 U/mL penicillin-streptomycin), and the concentration was adjusted.

Platelet Activation

Platelets were activated by 10 minutes of incubation at 37°C with 0.15 U/mL of thrombin and then neutralized by the addition of 2 U/mL hirudin.

Flow cytometric analysis was performed to confirm activation of the platelets by detecting P-selectin expressed on the platelet membranes.

Activated platelets and inactivated platelets were resuspended in phosphate-buffered saline (PBS) with 1% BSA and concentrated to 1×10^8/mL. Platelets were mixed with an equal volume of EDTA (final concentration 0.1%) and fixed for 30 minutes with 7.5% paraformaldehyde. After fixation, platelets were washed with PBS contained 2% BSA for 1 hour at room temperature. A PE-labeled mouse antihuman monoclonal antibody against CD62P was used in the flow cytometric analysis. Washed platelets were incubated with the PE-labeled antibody to CD62P for 20 minutes in the dark at room temperature. These samples were analyzed on a flow cytometer (JASCO Corporation, Tokyo, Japan) with an argon laser generating 488 nm, 10 mW. Inactivated platelets incubated

with the PE-labeled antibody to CD62P served as negative controls. The fluorescence intensity channel was set as 99.6%–99.9% of cells were within the negative area.

Chemoinvasion Assay

A chemoinvasion assay was performed to evaluate platelet-related promotion of invasiveness of tumor cells. The 5 tumor cell lines described above were prepared and adjusted to a concentration of 1.25×10^5 cells/mL. Activated and inactivated platelets were prepared to a final concentration 1.0×10^8/mL. Fibronectin was used as the chemoattractant. Three conditions of incubation media were compared for tumor cells only, tumor cells incubated with inactivated platelets, and tumor cell incubated with activated platelets.

A Matrigel basement membrane matrix was diluted with PBS and concentrated to 100 μg/mL. Diluted Matrigel was infused in BioCoat Cell Culture Inserts and incubated for 3 hours at 37°C and then desiccated overnight under a cell culture hood and at room temperature.

At the time of use, coated culture inserts with Matrigel were rehydrated for 2 hours with TC medium at room temperature; 750 μL of 50 μg/mL fibronectin was placed in each well of Falcon companion plates (under chambers) as the chemoattractant source.

After discarding the superfluous TC medium, 400 μL of tumor cell solution (final concentration 5.0×10^4/mL) was placed in the culture insert (upper chamber). One hundred microliters of TC medium (negative control), inactivated platelets, and activated platelets were added to the upper chamber.

After incubation for 24 hours at 37°C in 5% CO_2 atmosphere, cells that had invaded the lower surface of the filters were fixed and stained with a Diff-Quick stain kit. The cells were counted per microscopic field (×200). Five fields were counted in each of 3 different experiments.

Gelatin Zymography

A gelatin zymography electrophoresis kit was used for this analysis. The 5 pancreatic tumor cell lines were used. The samples were compared between 3 different solution conditions: tumor cells only, tumor cells with inactivated platelets, and tumor cells with activated platelets. The samples were incubated without or with inactivated platelets or with activated platelets for 24 hours at 37°C. Each 10 μL of samples was homogenized in 10 μL of sample buffer. Individual samples (10 μL) were electrophoresed at 10 mA for 20 minutes and then 20 mA for 80 minutes. The lower gels were washed twice for 30 minutes in 2.5% Triton X-100 to remove SDS, incubated for 24 hours in 50 mmol/L Tris-HCl buffer, pH 8.0, containing 0.5 mmol/L $CaCl_2$ at 37°C. Then gels were stained with 1% of Coomassie brilliant blue R-250 containing 10% methanol and 5% acetic acid for 30 minutes and destained with the same solution without Coomassie brilliant blue. Clear zones of gelatin lysis against a blue background stain after destaining indicated the presence of an enzyme. The densities of the observed bands were analyzed using NIH image 1.62 software (National Institutes of Health, Bethesda, MD). The 92-kd intensity ratio was calculated as the MMP-9 activity.

Western Blot Analysis

BxPC-3 was chosen as the mandated cell line for analysis because the invasiveness was most accelerated in the presence of platelets under the chemoinvasion assay. The samples were compared between the 3 different conditions described above. Conditioned samples were electrophoresed on multigel for 120 minutes at 40 mA and electrophoretically transferred to a nitrocellulose membrane for 120 minutes at 100 V. Blots were preblocked overnight in blocking solution (PBS, 0.1% Tween 20 containing 5% dried nonfat milk). After blocking, the blots were washed twice in PBS-T (PBS containing 0.1% Tween 20) for 15 minutes. The blots were incubated for 1 hour with the first antibody (antihuman MMP-9, purified IgG) diluted 1:100 with PBS-T. After two washings, they were incubated for 1 hour with the second antibody (antimouse IgG antibody) diluted 1:5000 with PBS-T, containing streptavidin/horseradish peroxidase conjugate. Bands were visualized by a chemiluminescence reaction using the ECL Western blotting system.

The Effects of Antiplatelet Agents

Three antiplatelet agents, PGI_2, EPA, and cilostazol were used in this study. The chemoinvasion assay was performed in the same manner as above using BxPC-3 to evaluate the antiplatelet effect, but among the following 5 different concentrations of media based on different concentrations of antiplatelet agents: 0, 1.25, 2.5, 5.0, and 10.0 μmol/L in PG I_2 and EPA and 0, 1.0, 2.5, 5.0, and 10.0 μg/mL in cilostazol.

Furthermore, we performed an ELISA assay for the quantitative determination of MMP-9 from tumor cells with or without platelets using BxPC-3 and cilostazol as antiplatelet agents because cilostazol inhibited the invasiveness of BxPC-3 in spite of the presence of platelets. The effect of cilostazol was compared for 5 different concentrations: 0, 1.0, 2.5, 5.0, and 10.0 μg/mL. Zero standard, each standard, and samples were pipetted into wells. After incubating for 1 hour at 25°C, the plate was washed 4 times with 0.01 mol/L phosphate buffer, pH 7.0, containing 0.05% Tween 20. Anti–MMP-9 horseradish peroxidase in 0.01 mol/L PBS (containing 1% BSA, 10 mmol/L EDTA, and 100 mmol/L sodium chloride) was added to all wells. After incubation for 2 hours at 25°C, the plate was washed 4 times. TMB substrate (3,3′,5,5′-tetramethylbenzidine) in dimethylformamide was added to all wells, and the plate was incubated for 20 minutes at room temperature on a plate shaker. The optical density of each well was measured.

Statistical Analysis

The results were expressed as mean ± SE of the indicated number of experiments. The data were analyzed by the Student

t test for paired samples. Statistical significance was set at $P < 0.05$.

RESULTS

Confirmation of activated Platelets

The number of CD62P-positive platelets in thrombin-activated platelets was studied by flow cytometry. The ratio of CD62P-positive platelets was compared between inactivated platelets (negative control) and thrombin-activated platelets (Fig. 1). The percentage of CD62P positive cells was 2.4% in inactivated platelets. In vitro activation with thrombin resulted in 76.4% CD62P-positive platelets. It was obvious that the number of CD62P-positive platelets in thrombin-activated platelets was greater than in inactivated platelets. Moreover, it was ascertained that inactivated platelets were not stimulated while platelets were washed.

Chemoinvasion Assay

An example of the chemoinvasion assay using the human pancreatic adenocarcinoma cell line SW.1990 is shown in Figure 2, comparing tumor cells only, incubation with inactivated platelets, and activated platelets. The number of tumor cells infiltrating to the lower side of the filter obviously increased in the presence of platelets.

All tumor cell lines showed that their capacity to traverse the matrigel was greatly increased when incubated with platelets. When incubated without platelets, the range of counted tumor cells was 2.8–8.8 cells/view. Under the condition of incubation with inactive platelets, the range of counted tumor cells was 10.3–50.4 cells/view and under incubation with activated platelets, they were 18.6–122.1 cells/view (Fig. 3). Especially in SW.1990 and BxPC-3, the number of cells greatly increased when incubated with inactivated platelets or with activated platelets (for SW.1990: without platelets, with inactive platelets, and with activated platelets were, respectively, 3.3, 26.9, and 58.2 cells/view; for BxPC-3: the respective values were 2.9, 50.3, and 122.1 cells/view). There were significant differences for both cell lines between the 3 different conditions of medium ($P < 0.01$).

Gelatin Zymography

The 5 pancreatic adenocarcinoma cell lines were used. The typical zymographic patterns of BxPC-3 are shown in Figure 4. In this figure, white broad bands of gelatin lysis were detected on 92 kd against a blue background. These bands meant the presence of the latent form of MMP-9 (pro–MMP-9). When tumor cells were incubated with platelets for 24 hours (either inactivated platelets or activated platelets), the intensity of the MMP-9 lysis band greatly increased compared with tumor cell with and without platelets (tumor cells only).

The zymographic profiles of gels were transilluminated, scanned, and then analyzed with NIH 1.62 image analysis software. MMP-9 activity was measured as the integrated area under the peak bands of the densitometric curve, and the 92-kd intensity ratio was calculated as the MMP-9 activity ratio. Under platelet-free conditions, the 92-kd intensity ratios were 4–61. On the other hand, under conditions of incubation with inactivated and activated platelets, the ratios were 77–313 and 100–322, respectively. In all cell lines, the intensity ratios of MMP-9 obviously increased when tumor cells were incubated with platelets, compared with without platelets (Fig. 5). Moreover, the intensities of MMP-9 bands of samples incubated with activated platelets were greater than samples incubated with inactivated platelets in all cell lines.

Western Blot Analysis

Western blot analysis was performed to confirm whether the bands detected in the gelatin zymography were actually MMP-9. The results of the Western blot analysis for MMP-9 in BxPC-3 are shown in Figure 6, in which bands of the latent form of MMP-9 can be detected (92 kd). The band on the lane of the sample incubated with activated platelets is obviously greater than the sample with inactivated platelets. Furthermore, the band of inactivated platelets was increased compared with the sample without platelets.

Effects of Antiplatelet Agents

To evaluate the effect of antiplatelet agents on platelet-related promotion of BxPC-3 invasiveness by platelets, the chemoinvasion assay was performed again under incubation

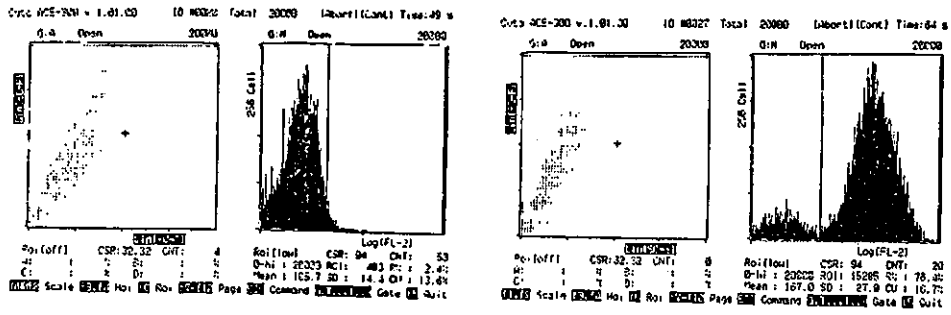

A: Inactivated platelets (negative control)

B: Activated platelets

FIGURE 1. Flow cytometric analysis of inactivated platelets and thrombin-activated platelets. The percentage of CD62P-positive cells was 2.4% in inactivated platelets (A). In activated platelets with thrombin, the percentage of CD62P-positive cells was 76.4%. It was ascertained that activated platelets were stimulated by thrombin and that inactivated platelets were not stimulated while the platelets were washed.